Deciphering twist-3 chiral-even GPDs in the light-front quark-diquark model

Sameer Jain,[*] Shubham Sharma,[†] and Harleen Dahiya[‡]

Department of Physics, Dr. B. R. Ambedkar National Institute of Technology, Jalandhar, 144008, India

(Received 9 August 2024; accepted 14 October 2024; published 15 November 2024)

We investigate quantum chromodynamics (QCD) in this study by computing chiral-even generalized parton distributions (GPDs) at twist-3 in the framework of the light-front quark-diquark model, particularly in the zero skewness scenario. We provide a detailed examination of twist-3 chiral-even GPDs, illustrating their behavior through extensive two-dimensional (2-D) and three-dimensional (3-D) visualizations, which demonstrate their dependence on the longitudinal momentum fraction (x) and the momentum transfer (t). Our investigation also reveals the intricate relationships between these GPDs and other distribution functions such as generalized transverse-momentum dependent distributions, transverse momentum-dependent parton distributions, and parton distribution functions (PDFs). Our study also includes the connected form factors at this twist, which are crucial in understanding the internal structure of hadrons. Additionally, we provide impact parameter-dependent PDF plots to offer insights into the spatial distribution of partons.

DOI: 10.1103/PhysRevD.110.094030

I. INTRODUCTION

The proton is among the first particles to be discovered experimentally, yet even after a century, its structure remains elusive [1]. The "proton spin crisis" has intrigued researchers for decades, and the "origin of proton mass" is a highly active field of research, encompassing both experimental and theoretical investigations [2–12]. Experimental facilities such as the Stanford Linear Accelerator Center [13–18], the European Organization for Nuclear Research [19–24], the Deutsches Elektronen-Synchrotron [25–27], and Jefferson Lab [28–32] have played crucial roles in the aforementioned studies. The usual approach of analyzing the proton's structure includes scattering experiments, with deep inelastic scattering (DIS) being a key method [33–35]. Using the factorization theorem, the cross section of DIS is parametrized in terms of parton distribution functions (PDFs), which are quasiprobabilistic distributions providing information about the partons, i.e., quarks or gluons, inside the proton [36–38]. Although at very short distances, i.e., at very high energies, perturbative quantum chromodynamics (QCD) provides significant results by adding leading order, next-to-leading order, and higher-order corrections [39,40], at low energies, factorization theorems are not as effective [41]. Moreover, nonperturbative effects become dominant. To gain a clearer understanding of a proton's structure at low energies, it is necessary to consider additional corrections, including target mass corrections and higher twist corrections [42–44].

Information obtained from PDFs is fairly restricted as it acknowledges only the one-dimensional (1D) distribution of the longitudinal momentum fraction x of the parton. Higher-dimensional distributions such as transverse momentum distributions (TMDs) provide more information concerning the proton's three-dimensional (3D) configuration using kinematic variables such as x and the transverse momentum of the parton $p_\perp$ [33,34,45–72]. TMDs correspond to phenomena of semi-inclusive deep inelastic scattering and Drell-Yan [73–88]. Another higher-dimensional distribution, generalized parton distributions (GPDs), are parametrized in the variables x and momentum transfer to the proton $\boldsymbol{\Delta}_\perp$. Such distributions correspond to scattering processes such as deeply virtual Compton scattering (DVCS) and deeply virtual meson production (DVMP) [89–106]. Even higher-dimensional distributions, such as generalized transverse momentum distributions (GTMDs), carry the most information about the parton [107]. The relationship between the previously discussed distributions, along with some other distributions, can be seen in Fig. 1.

GPDs appear while studying the cross-section of scattering processes such as DVCS and DVMP. They are also known as the nonforward matrix elements of bilocal operators in such processes. Although direct extraction of GPDs from sophisticated experiments such

[*]Contact author: sameerjainofficial@gmail.com
[†]Contact author: s.sharma.hep@gmail.com
[‡]Contact author: dahiyah@nitj.ac.in

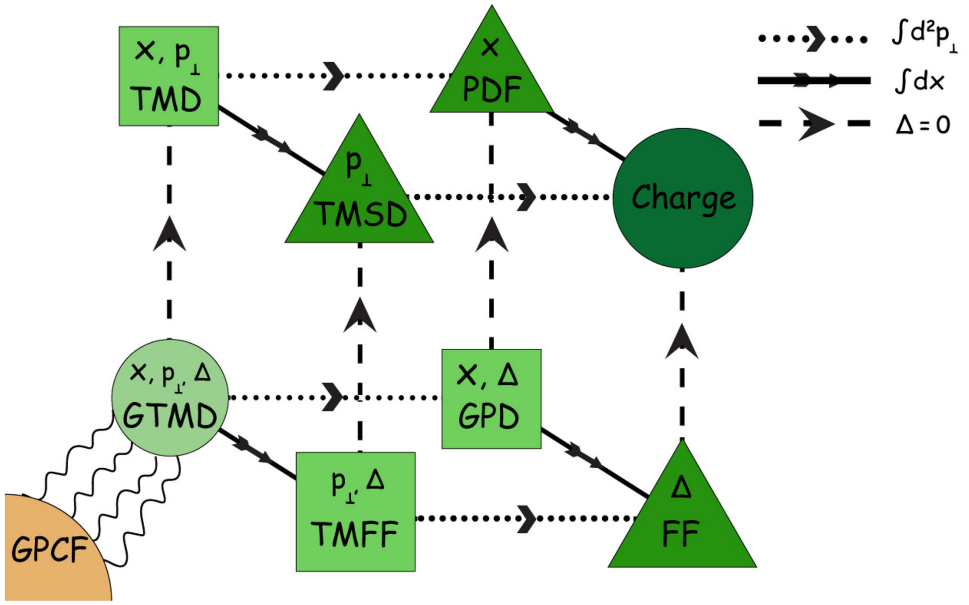

FIG. 1. A illustration of the generalized parton correlation functions (GPCFs) using family trees. Various arrows represent various GTMD limits. The dashed line represents the case of zero momentum transfer, the solid line represents the integration over the longitudinal momentum fraction x, and the dotted line shows the integration over the quark's transverse momentum $\mathbf{p}_\perp$ [108].

as Zentrum für Elektronen-Und-Speicherringexperiment [109,110], CEBAF large acceptance spectrometer (CLAS) [111–118], and common muon and proton apparatus (COMPASS) [119] is not straightforward, it becomes even more complicated when we consider higher twist corrections [120,121]. References [122,123] suggest that twist-3 GPDs can provide vital information about a quark's kinetic orbital angular momentum and quark spin-orbit interactions. The Fourier transform of GPDs provides the impact parameter dependent parton distribution functions (IPDPDFs), which are functions of x and the impact parameter distance $\mathbf{b}_\perp$ [124]. IPDPDFs offer the most physical picture of the proton as they suggest the position of partons, giving a familiar understanding of the structure of an object.

One of the most successful and profound theories in the history of physics, offering explanations for physical phenomena with unparalleled accuracy, particularly in the realm of high-energy physics, is quantum field theory (QFT). The remarkable achievements of QFT are best illustrated by QCD, the theory of quark-gluon interactions [125]. However, achieving this level of accuracy presents tremendous computational challenges that require sophisticated methods and adjustments that consider various effects. One mathematical approach to simplifying computations in QCD is the use of anti–de Sitter (AdS)/QCD correspondence. This method, along with Dirac's light-front dynamics, can dramatically simplify calculations and provide more familiarity with the underlying physics [126]. The light-front quark-diquark model (LFQDM) serves as a model that uses both of these mathematical formulations along with the assumption that during interactions with a probe, the proton acts as a composite of an active quark participating in the interaction while the remaining quarks form a spectator diquark [127–129]. In recent years, LFQDM has accomplished many significant results. For example, it has shown very promising results for spin asymmetry, aiding in the study of experiments like hadron-elektron ring anlage measurement of spin and COMPASS [130]. The flavor combination of the PDF $e(x)$ compares nicely with the CLAS data [130]. Multiple properties of the proton, such as mechanical radius, shear forces, and pressure distributions, along with structure functions such as gravitational form factors (FFs) and transversity and helicity PDFs, have been calculated using LFQDM [131]. Recent works also include calculations of the transverse structure of the proton in Refs. [129,132,133]. Twist-2, twist-3, and twist-4 GTMDs are discussed in Refs. [108,134,135], while twist-2 and twist-4 GPDs have been calculated in Refs. [136,137].

The objective of our work aims to analyze the twist-3 GPDs of protons within the LFQDM framework. Primarily, the unintegrated quark-quark GPD correlator has been deciphered for twist-3 Dirac matrix structure, and we then, through comparison with the parametrization equations, achieve the equations for the twist-3 GPDs of the proton. The explicit equations for GPDs have been derived for both possible scenarios of active quark flavor u and d from vector and scalar diquark components, considering a skewness ξ of 0. The nature of twist-3 chiral-even GPDs is illustrated using two-dimensional (2D) and 3D graphs, depicting their dependency over a quark's longitudinal momentum fraction

x and the momentum transfer t. To unify the obtained findings of this study and their connections with other distribution functions, we seek the associated GTMDs, TMDs, and PDFs. We have included the analysis of associated GPDs in impact parameter space, obtained through the Fourier transformation of GPDs. Additionally, twist-3 FFs have also been discussed considering their significance for the comprehension of proton dynamics.

The article has adopted the following structure: The LFQDM's crucial details, input parameters, and other constants are discussed in Sec. II. The twist-3 quark-quark GPD correlator features are covered in Sec. III, along with the pertinent parametrization equations. The explicit equations for twist-3 GPDs are shown in Sec. IV. A sequential analysis of the relationships between twist-3 chiral-even GPDs with GTMDs and TMDs is presented in Secs. V and VI respectively. A 2D and 3D plot-based analysis of GPDs is presented in Sec. VII. This section also covers Fourier-transformed GPD illustrations and twist-3 FFs. Finally, a conclusion is presented in Sec. VIII.

II. LFQDM

Regarding the LFQDM explanation, for an all-encompassing perspective on the probability of running into every possible active quark-spectator combination, the proton's spin-flavor structure is thought to be composed of isoscalar-scalar diquark singlet $|uS^0\rangle$, isoscalar-vector diquark $|uA^0\rangle$, and isovector-vector diquark $|dA^1\rangle$ states from Ref. [127]:

$$|P;\Lambda^N\rangle = C_S|uS^0\rangle^{\Lambda^N} + C_V|uA^0\rangle^{\Lambda^N} + C_{VV}|dA^1\rangle^{\Lambda^N}. \quad (1)$$

In the above expression, the nucleon helicity is Λ^N. The spinwise vector and scalar diquark parts are denoted by $A = V, VV$ and S, respectively. The diquarks' respective isospins have been indicated by the superscripts (0) or (1). The coefficients C_i of scalar and vector diquark states have been found in Ref. [127] and are provided in Table II. The valence quark's proportion of longitudinal momentum from the parent proton is $x = p^+/P^+$, where the momentum of quark (p) and diquark (P_X) is given as

$$p \equiv (xP^+, p^-, \mathbf{p}_\perp), \quad (2)$$

$$P_X \equiv ((1-x)P^+, P_X^-, -\mathbf{p}_\perp), \quad (3)$$

for the case when proton carries no transverse momenta. The expansion of the Fock state for $J^z = \pm 1/2$ for the scalar $|\nu S\rangle^{\Lambda^N}$ and vector diquark $|\nu A\rangle^{\Lambda^N}$ in the case of two particles can be expressed as [129,138,139]

$$|\nu S\rangle^{\pm} = \sum_{\lambda^q}\int \frac{dxd^2\mathbf{p}_\perp}{2(2\pi)^3\sqrt{x(1-x)}}\psi^{\pm(\nu)}_{\lambda^q}(x,\mathbf{p}_\perp)|\lambda^q,\lambda^S;xP^+,\mathbf{p}_\perp\rangle, \quad (4)$$

$$|\nu A\rangle^{\pm} = \sum_{\lambda^q}\sum_{\lambda^D}\int \frac{dxd^2\mathbf{p}_\perp}{2(2\pi)^3\sqrt{x(1-x)}}\psi^{\pm(\nu)}_{\lambda^q\lambda^D}(x,\mathbf{p}_\perp)|\lambda^q,\lambda^D;xP^+,\mathbf{p}_\perp\rangle. \quad (5)$$

The flavor index $\nu = u$ (for the scalar case) and $\nu = u, d$ (for the vector case) are determined using Eq. (1). The two particle state is represented by the expression $|\lambda^q,\lambda^{Sp};xP^+,\mathbf{p}_\perp\rangle$, where the quark helicity is $\lambda^q = \pm\frac{1}{2}$ and the spectator diquark helicity is λ^{Sp}. The scalar diquark's spectator helicity is $\lambda^{Sp} = \lambda^S = 0$ (singlet), while the vector diquark's spectator helicity is $\lambda^{Sp} = \lambda^D = \pm 1, 0$ (triplet). Table I provides the LFWFs [129] for $J^z = \pm 1/2$, taking into account the scalar or vector nature of diquarks. Derived from the predictions of soft-wall AdS/QCD [140,141], the general form of LFWFs $\varphi_i^{(\nu)} = \varphi_i^{(\nu)}(x,\mathbf{p}_\perp)$ listed in Table I follows the parametrization a_i^ν, b_i^ν, and δ^ν as outlined in Ref. [127]. We have

$$\varphi_i^{(\nu)}(x,\mathbf{p}_\perp) = \frac{4\pi}{\kappa}\sqrt{\frac{\log(1/x)}{1-x}}x^{a_i^\nu}(1-x)^{b_i^\nu} \times \exp\left[-\delta^\nu\frac{\mathbf{p}_\perp^2}{2\kappa^2}\frac{\log(1/x)}{(1-x)^2}\right]. \quad (6)$$

The wave functions φ_i^ν $(i = 1, 2)$ happen to be distinct over the interchange $x \to 1-x$, and such asymmetry persists at the AdS/QCD limit $a_i^\nu = b_i^\nu = 0$ and $\delta^\nu = 1.0$ as well [142].

The variables a_i^ν and b_i^ν, appearing in Eq. (6), were effectively fitted with the use of the Dirac and Pauli FF data [127,143,144] to the model scale $\mu_0 = 0.313$ GeV. For both quark flavors, the given value of factor δ^ν is assumed as the one that has been adopted from AdS/QCD [140]. Aside from this, Ref. [127] is the source of normalization constants N_i^2 provided in Table I. Table II lists the model parameter values for both active quark flavors, considering the purpose of clarity. The AdS/QCD scale parameter κ, which appears in Eq. (6), has been assigned a value of 0.4 GeV [145,146]. We take the proton mass (M) and the constituent quark mass (m) to be, respectively, 0.938 GeV and 0.055 GeV, consistent with Ref. [128]. By considering the contributions from isoscalar-scalar ($O^{u(S)}$), isoscalar vector ($O^{u(V)}$), and isovector-vector ($O^{d(VV)}$), parts, we can write any physical observable O for active u and d quarks as

TABLE I. The LFWFs for the active quark λ^q and the spectator diquark λ^{Sp} variations of their helicities for both diquark circumstances for $J^z = \pm 1/2$. The normalization constants are N_S, $N_0^{(\nu)}$, and $N_1^{(\nu)}$.

Diquark	λ^q	λ^{Sp}	LFWFs for $J^z = +1/2$		LFWFs for $J^z = -1/2$	
Scalar	$+1/2$	0	$\psi_+^{+(\nu)}$	$= N_S \varphi_1^{(\nu)}$	$\psi_+^{-(\nu)}$	$= N_S(\frac{p^1 - ip^2}{xM})\varphi_2^{(\nu)}$
	$-1/2$	0	$\psi_-^{+(\nu)}$	$= -N_S(\frac{p^1 + ip^2}{xM})\varphi_2^{(\nu)}$	$\psi_-^{-(\nu)}$	$= N_S \varphi_1^{(\nu)}$
Vector	$+1/2$	$+1$	$\psi_{++}^{+(\nu)}$	$= N_1^{(\nu)}\sqrt{\frac{2}{3}}(\frac{p^1 - ip^2}{xM})\varphi_2^{(\nu)}$	$\psi_{++}^{-(\nu)}$	$= 0$
	$-1/2$	$+1$	$\psi_{-+}^{+(\nu)}$	$= N_1^{(\nu)}\sqrt{\frac{2}{3}}\varphi_1^{(\nu)}$	$\psi_{-+}^{-(\nu)}$	$= 0$
	$+1/2$	0	$\psi_{+0}^{+(\nu)}$	$= -N_0^{(\nu)}\sqrt{\frac{1}{3}}\varphi_1^{(\nu)}$	$\psi_{+0}^{-(\nu)}$	$= N_0^{(\nu)}\sqrt{\frac{1}{3}}(\frac{p^1 - ip^2}{xM})\varphi_2^{(\nu)}$
	$-1/2$	0	$\psi_{-0}^{+(\nu)}$	$= N_0^{(\nu)}\sqrt{\frac{1}{3}}(\frac{p^1 + ip^2}{xM})\varphi_2^{(\nu)}$	$\psi_{-0}^{-(\nu)}$	$= N_0^{(\nu)}\sqrt{\frac{1}{3}}\varphi_1^{(\nu)}$
	$+1/2$	-1	$\psi_{+-}^{+(\nu)}$	$= 0$	$\psi_{+-}^{-(\nu)}$	$= -N_1^{(\nu)}\sqrt{\frac{2}{3}}\varphi_1^{(\nu)}$
	$-1/2$	-1	$\psi_{--}^{+(\nu)}$	$= 0$	$\psi_{--}^{-(\nu)}$	$= N_1^{(\nu)}\sqrt{\frac{2}{3}}(\frac{p^1 + ip^2}{xM})\varphi_2^{(\nu)}$

TABLE II. Values of coefficients, normalization constants N_i^2, and model parameters corresponding to both u and d quarks.

Parameter		
ν	u	d
C_S^2	1.3872	0
C_V^2	0.6128	0
C_{VV}^2	0	1
N_S	2.0191	0
N_0^ν	3.2050	5.9423
N_1^ν	0.9895	1.1616
a_1^ν	0.280 ± 0.001	0.5850 ± 0.0003
b_1^ν	0.1716 ± 0.0051	0.7000 ± 0.0002
a_2^ν	0.84 ± 0.02	$0.9434^{+0.0017}_{-0.0013}$
b_2^ν	0.2284 ± 0.0035	$0.64^{+0.0082}_{-0.0022}$
δ^ν	1	1

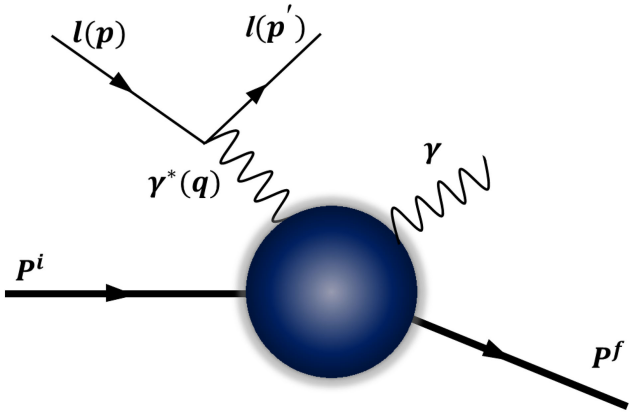

FIG. 2. Visualization of the GPDs-linked DVCS process involving a virtual photon and proton, $\gamma^* + P^i \to \gamma^* + P^f$.

$$O^u = O^{u(S)} + O^{u(V)}, \tag{7}$$

$$O^d = O^{d(VV)}. \tag{8}$$

III. GPD CORRELATOR AND PARAMETRIZATION AT TWIST-3

This section presents a thorough examination of the GPD correlator and its parametrization. According to Ref. [147], the quark-quark GPD correlator for the proton is defined as

$$F^{\nu[\Gamma]}_{[\Lambda^{N_i}\Lambda^{N_f}]}(x,\xi,t) = \frac{1}{2}\int \frac{dz^-}{2\pi} e^{\frac{i}{2}p^+z^-}\langle P^f;\Lambda^{N_f}|\bar{\psi}(-z/2) \times \Gamma \mathcal{W}_{[-z/2,z/2]}\psi(z/2)|P^i;\Lambda^{N_i}\rangle|_{z^+=z_\perp=0}. \tag{9}$$

In the present work, $|P^i;\Lambda^{N_i}\rangle$ and $|P^f;\Lambda^{N_f}\rangle$ represent the initial and final states of the proton, respectively, where Λ^{N_i} and Λ^{N_f} signify their helicities. The pictorial representation of the GPDs-linked DVCS process $\gamma^* + P^i \to \gamma^* + P^f$, involving a virtual photon and proton where a virtual photon is observed in the final state along with the proton, has been given in Fig. 2. The GPD correlator depends on the variables set x, ξ, and t. At zero skewness, the square of the total momentum transfer is denoted by $t = \Delta^2 = -\boldsymbol{\Delta}_\perp^2$, or $\xi = -\Delta^+/2P^+ = 0$ [147]. Therefore, for the rest of the paper, we will express the GPD correlator $F^{\nu[\Gamma]}_{[\Lambda^{N_i}\Lambda^{N_f}]}(x,\xi,t)$ as $F^{\nu[\Gamma]}_{[\Lambda^{N_i}\Lambda^{N_f}]}(x,\boldsymbol{\Delta}_\perp^2)$ or compactly as $F^{\nu[\Gamma]}_{[\Lambda^{N_i}\Lambda^{N_f}]}$, where Γ stands for the twist-3 Dirac γ matrices, i.e., $\Gamma = \{\gamma^j, \gamma^j\gamma_5\}$. The Wilson line, $\mathcal{W}_{[-z/2,z/2]}$, has been considered to be 1 for simplicity. This ensures that the related bilocal quark operator has SU(3) color gauge invariance. In the present scenario, we use the convention $z^\pm = (z^0 \pm z^3)$, and we

apply the symmetric frame kinematics that has been adopted in Ref. [136].

By substituting the expression of the scalar diquark and vector diquark Fock states, Eqs. (4) and (5), into the proton state Eq. (1) within the GPD correlator, Eq. (9), one can get the GPD correlator for the scalar and vector diquark parts as an overlap of LFWFs, shown in Table I as

$$F^{\nu[\Gamma](S)}_{[\Lambda^{N_i}\Lambda^{N_f}]}(x,\mathbf{\Delta}_\perp^2) = \int \frac{C_S^2}{16\pi^3}\sum_{\lambda^{q_i}}\sum_{\lambda^{q_f}} \psi^{\Lambda^{N_f}\dagger}_{\lambda^{q_f}}\left(x,\mathbf{p}_\perp+(1-x)\frac{\mathbf{\Delta}_\perp}{2}\right)\psi^{\Lambda^{N_i}}_{\lambda^{q_i}}\left(x,\mathbf{p}_\perp-(1-x)\frac{\mathbf{\Delta}_\perp}{2}\right) \times \frac{u^\dagger_{\lambda^{q_f}}(xP^+,\mathbf{p}_\perp+\frac{\mathbf{\Delta}_\perp}{2})\gamma^0\Gamma u_{\lambda^{q_i}}(xP^+,\mathbf{p}_\perp-\frac{\mathbf{\Delta}_\perp}{2})}{2xP^+}d^2\mathbf{p}_\perp, \tag{10}$$

$$F^{\nu[\Gamma](A)}_{[\Lambda^{N_i}\Lambda^{N_f}]}(x,\mathbf{\Delta}_\perp^2) = \int \frac{C_A^2}{16\pi^3}\sum_{\lambda^{q_i}}\sum_{\lambda^{q_f}}\sum_{\lambda^D} \psi^{\Lambda^{N_f}\dagger}_{\lambda^{q_f}\lambda^D}\left(x,\mathbf{p}_\perp+(1-x)\frac{\mathbf{\Delta}_\perp}{2}\right)\psi^{\Lambda^{N_i}}_{\lambda^{q_i}\lambda^D}\left(x,\mathbf{p}_\perp-(1-x)\frac{\mathbf{\Delta}_\perp}{2}\right) \times \frac{u^\dagger_{\lambda^{q_f}}(xP^+,\mathbf{p}_\perp+\frac{\mathbf{\Delta}_\perp}{2})\gamma^0\Gamma u_{\lambda^{q_i}}(xP^+,\mathbf{p}_\perp-\frac{\mathbf{\Delta}_\perp}{2})}{2xP^+}d^2\mathbf{p}_\perp, \tag{11}$$

where $C_A = C_V, C_{VV}$ for the u and d quarks, respectively. The spinor product $u^\dagger_{\lambda^{q_f}}(xP^+,\mathbf{p}_\perp+\frac{\mathbf{\Delta}_\perp}{2})\,\gamma^0\Gamma u_{\lambda^{q_i}}(xP^+,\mathbf{p}_\perp-\frac{\mathbf{\Delta}_\perp}{2})$ is associated with the twist-3 Dirac matrices. References [125,126] provide a comprehensive discussion of the various Dirac spinor configurations. Here, λ^{q_i} and λ^{q_f} stand for initial and final states of the quark helicity, respectively. Moreover, for the vector diquark, there is an extra summation over the diquark helicity λ^D.

Following Ref. [147], the GPDs connected to the twist-3 Dirac matrices γ^j and $\gamma^j\gamma_5$ can be parametrized as

$$F^{[\gamma^j]}_{[\Lambda^{N_i}\Lambda^{N_f}]} = \frac{M}{2(P^+)^2}\bar{u}(P^f,\Lambda^{N_f})\Big[i\sigma^{+j}H_{2T}(x,\mathbf{\Delta}_\perp^2)+\frac{\gamma^+\mathbf{\Delta}^j_\perp-\Delta^+\gamma^j}{2M}E_{2T}(x,\mathbf{\Delta}_\perp^2) + \frac{P^+\mathbf{\Delta}^j_\perp-\Delta^+\mathbf{P}^j_\perp}{M^2}\tilde{H}_{2T}(x,\mathbf{\Delta}_\perp^2)+\frac{\gamma^+\mathbf{P}^j_\perp-P^+\gamma^j}{M}\tilde{E}_{2T}(x,\mathbf{\Delta}_\perp^2)\Big]u(P^i,\Lambda^{N_i}), \tag{12}$$

$$F^{[\gamma^j\gamma_5]}_{[\Lambda^{N_i}\Lambda^{N_f}]} = -\frac{i\varepsilon^{ij}_\perp M}{2(P^+)^2}\bar{u}(P^f,\Lambda^{N_f})\Big[i\sigma^{+i}H'_{2T}(x,\mathbf{\Delta}_\perp^2)+\frac{\gamma^+\mathbf{\Delta}^i_\perp-\Delta^+\gamma^i}{2M}E'_{2T}(x,\mathbf{\Delta}_\perp^2) + \frac{P^+\mathbf{\Delta}^i_\perp-\Delta^+\mathbf{P}^i_\perp}{M^2}\tilde{H}'_{2T}(x,\mathbf{\Delta}_\perp^2)+\frac{\gamma^+\mathbf{P}^i_\perp-P^+\gamma^i}{M}\tilde{E}'_{2T}(x,\mathbf{\Delta}_\perp^2)\Big]u(P^i,\Lambda^{N_i}). \tag{13}$$

Here, the chiral-even GPDs are represented by functions of the form $X(x,\mathbf{\Delta}_\perp^2)$, which are eight in number. In the above expressions, we have used the relation $\sigma^{+\Delta} = \sigma^{+i}\Delta_i$ for transverse direction index i, whereas other notations have their usual meanings.

IV. EXPRESSIONS OF TWIST-3 CHIRAL-EVEN GPDS

To derive the expressions of the twist-3 chiral-even GPDs for each kind of diquark, we have substituted the proton state, Eq. (1), with proper polarization in the correlator, Eq. (9), via scalar and vector diquark Fock states from Eqs. (4) and (5), respectively. One can obtain certain twist-3 chiral-even GPDs by choosing the matrix structure $\Gamma = \gamma^j$ from Eq. (12):

$$\frac{i\mathbf{\Delta}_\perp^2}{P^+}\tilde{E}^\nu_{2T} = \Delta_y\left(F^{\nu[\gamma^1]}_{[++]}-F^{\nu[\gamma^1]}_{[--]}\right)-\Delta_x\left(F^{\nu[\gamma^2]}_{[++]}-F^{\nu[\gamma^2]}_{[--]}\right), \tag{14}$$

$$\frac{-2iM\mathbf{\Delta}_\perp^2}{P^+}H^\nu_{2T} = (\Delta_x+i\Delta_y)\left(\Delta_y F^{\nu[\gamma^1]}_{[-+]}-\Delta_x F^{\nu[\gamma^2]}_{[-+]}\right) + (\Delta_x-i\Delta_y)\left(\Delta_y F^{\nu[\gamma^1]}_{[+-]}-\Delta_x F^{\nu[\gamma^2]}_{[+-]}\right), \tag{15}$$

$$\frac{4M^2H^\nu_{2T}+\tilde{H}^\nu_{2T}\mathbf{\Delta}_\perp^2}{MP^+} = \left(F^{\nu[\gamma^1]}_{[-+]}-F^{\nu[\gamma^1]}_{[+-]}\right)+i\left(F^{\nu[\gamma^2]}_{[-+]}+F^{\nu[\gamma^2]}_{[+-]}\right), \tag{16}$$

$$\frac{2(\mathbf{p}_\perp\cdot\mathbf{\Delta}_\perp)\tilde{E}^\nu_{2T}+(E^\nu_{2T}+2\tilde{H}^\nu_{2T})\mathbf{\Delta}_\perp^2}{P^+} = \Delta_x\left(F^{\nu[\gamma^1]}_{[++]}+F^{\nu[\gamma^1]}_{[--]}\right)+\Delta_y\left(F^{\nu[\gamma^2]}_{[++]}+F^{\nu[\gamma^2]}_{[--]}\right). \tag{17}$$

Similarly, for the matrix structure $\Gamma = \gamma^j\gamma_5$, we have obtained the following equations:

$$\frac{\boldsymbol{\Delta}_\perp^2}{P^+}\tilde{E}'^{\nu}_{2T} = \Delta_x\left(F^{\nu[\gamma^1\gamma_5]}_{[++]} - F^{\nu[\gamma^1\gamma_5]}_{[--]}\right) + \Delta_y\left(F^{\nu[\gamma^2\gamma_5]}_{[++]} - F^{\nu[\gamma^2\gamma_5]}_{[--]}\right), \tag{18}$$

$$\frac{2M\boldsymbol{\Delta}_\perp^2}{P^+}H'^{\nu}_{2T} = (\Delta_x + i\Delta_y)\left(\Delta_x F^{\nu[\gamma^1\gamma_5]}_{[-+]} + \Delta_y F^{\nu[\gamma^2\gamma_5]}_{[-+]}\right) + (\Delta_x - i\Delta_y)\left(\Delta_x F^{\nu[\gamma^1\gamma_5]}_{[+-]}\Delta_y F^{\nu[\gamma^2\gamma_5]}_{[+-]}\right), \tag{19}$$

$$\frac{4M^2H'^{\nu}_{2T} + \tilde{H}'^{\nu}_{2T}\boldsymbol{\Delta}_\perp^2}{MP^+} = \left(F^{\nu[\gamma^1\gamma_5]}_{[-+]} + F^{\nu[\gamma^1\gamma_5]}_{[+-]}\right) + i\left(F^{\nu[\gamma^2\gamma_5]}_{[-+]} - F^{\nu[\gamma^2\gamma_5]}_{[+-]}\right), \tag{20}$$

$$i\frac{2(\mathbf{p}_\perp\cdot\boldsymbol{\Delta}_\perp)\tilde{E}'^{\nu}_{2T} + (E'^{\nu}_{2T} + 2\tilde{H}'^{\nu}_{2T})\boldsymbol{\Delta}_\perp^2}{P^+} = \Delta_y\left(F^{\nu[\gamma^1\gamma_5]}_{[++]} + F^{\nu[\gamma^1\gamma_5]}_{[--]}\right) - \Delta_x\left(F^{\nu[\gamma^2\gamma_5]}_{[++]} + F^{\nu[\gamma^2\gamma_5]}_{[--]}\right). \tag{21}$$

We define

$$T^{(\nu)}_{ij}(x,\mathbf{p}_\perp,\boldsymbol{\Delta}_\perp) = \varphi^{(\nu)\dagger}_i\left(x,\mathbf{p}_\perp + (1-x)\frac{\boldsymbol{\Delta}_\perp}{2}\right) \times \varphi^{(\nu)}_j\left(x,\mathbf{p}_\perp - (1-x)\frac{\boldsymbol{\Delta}_\perp}{2}\right), \tag{22}$$

where, $i, j = 1, 2$. By using the wave function from Eq. (6) with the aforementioned equation, one may infer

$$T^{(\nu)}_{ij}(x,\mathbf{p}_\perp,\boldsymbol{\Delta}_\perp) = T^{(\nu)}_{ji}(x,\mathbf{p}_\perp,\boldsymbol{\Delta}_\perp), \tag{23}$$

$$\varphi^{(\nu)\dagger}_i\left(x,\mathbf{p}_\perp + (1-x)\frac{\boldsymbol{\Delta}_\perp}{2}\right) = \varphi^{(\nu)}_i\left(x,\mathbf{p}_\perp + (1-x)\frac{\boldsymbol{\Delta}_\perp}{2}\right). \tag{24}$$

For the twist-3 Dirac matrix structure, the chiral-even GPD expressions for both diquark possibilities can be written as

$$x\tilde{E}^{\nu(S)}_{2T} = \int \frac{C_S^2N_s^2}{16\pi^3}\left(-T^\nu_{11} + \left(\left(\mathbf{p}_\perp^2 - (1-x)^2\frac{\boldsymbol{\Delta}_\perp^2}{4}\right) - 2\left(\frac{\mathbf{p}_\perp^2\boldsymbol{\Delta}_\perp^2 - (\mathbf{p}_\perp\cdot\boldsymbol{\Delta}_\perp)^2}{\boldsymbol{\Delta}_\perp^2}\right)(1-x)\right)\frac{T^\nu_{22}}{x^2M^2}\right)d^2\mathbf{p}_\perp, \tag{25}$$

$$x\tilde{E}^{\nu(A)}_{2T} = \int \frac{C_A^2}{16\pi^3}\left(\frac{1}{3}|N_0^\nu|^2 - \frac{2}{3}|N_1^\nu|^2\right)\left(-T^\nu_{11} + \left(\left(\mathbf{p}_\perp^2 - (1-x)^2\frac{\boldsymbol{\Delta}_\perp^2}{4}\right) - 2\left(\frac{\mathbf{p}_\perp^2\boldsymbol{\Delta}_\perp^2 - (\mathbf{p}_\perp\cdot\boldsymbol{\Delta}_\perp)^2}{\boldsymbol{\Delta}_\perp^2}\right)(1-x)\right)\frac{T^\nu_{22}}{x^2M^2}\right)d^2\mathbf{p}_\perp, \tag{26}$$

$$xH'^{\nu(S)}_{2T} = \int \frac{C_S^2N_s^2}{16\pi^3}\frac{1}{M}\left(mT^\nu_{11} + 2\frac{(\mathbf{p}_\perp\cdot\boldsymbol{\Delta}_\perp)^2}{\boldsymbol{\Delta}_\perp^2}\frac{T^\nu_{12}}{xM} - m\left(\left(\frac{2(\mathbf{p}_\perp\cdot\boldsymbol{\Delta}_\perp)^2 - \mathbf{p}_\perp^2\boldsymbol{\Delta}_\perp^2}{\boldsymbol{\Delta}_\perp^2}\right) - (1-x)^2\frac{\boldsymbol{\Delta}_\perp^2}{4}\right)\frac{T^\nu_{22}}{x^2M^2}\right)d^2\mathbf{p}_\perp, \tag{27}$$

$$xH'^{\nu(A)}_{2T} = \int -\frac{C_A^2}{16\pi^3}\left(\frac{1}{3}|N_0^\nu|^2\right)\frac{1}{M}\left(mT^\nu_{11} + 2\frac{(\mathbf{p}_\perp\cdot\boldsymbol{\Delta}_\perp)^2}{\boldsymbol{\Delta}_\perp^2}\frac{T^\nu_{12}}{xM} - m\left(\left(\frac{2(\mathbf{p}_\perp\cdot\boldsymbol{\Delta}_\perp)^2 - \mathbf{p}_\perp^2\boldsymbol{\Delta}_\perp^2}{\boldsymbol{\Delta}_\perp^2}\right) - (1-x)^2\frac{\boldsymbol{\Delta}_\perp^2}{4}\right)\frac{T^\nu_{22}}{x^2M^2}\right)d^2\mathbf{p}_\perp, \tag{28}$$

$$x\tilde{H}'^{\nu(S)}_{2T} = \int \frac{C_S^2N_s^2}{4\pi^3}\frac{M}{\boldsymbol{\Delta}_\perp^2}\left[\left(\left(\frac{\mathbf{p}_\perp^2\boldsymbol{\Delta}_\perp^2 - 2(\mathbf{p}_\perp\cdot\boldsymbol{\Delta}_\perp)^2}{\boldsymbol{\Delta}_\perp^2}\right) + (1-x)\frac{\boldsymbol{\Delta}_\perp^2}{4}\right)\frac{T^\nu_{12}}{xM} - m\left(\left(\frac{\mathbf{p}_\perp^2\boldsymbol{\Delta}_\perp^2 - 2(\mathbf{p}_\perp\cdot\boldsymbol{\Delta}_\perp)^2}{\boldsymbol{\Delta}_\perp^2}\right) + (1-x)^2\frac{\boldsymbol{\Delta}_\perp^2}{4}\right)\frac{T^\nu_{22}}{x^2M^2}\right]d^2\mathbf{p}_\perp, \tag{29}$$

$$x\tilde{H}'^{\nu(A)}_{2T} = \int -\frac{C_A^2}{4\pi^3}\left(\frac{1}{3}|N_0^\nu|^2\right)\frac{M}{\boldsymbol{\Delta}_\perp^2}\left[\left(\left(\frac{\mathbf{p}_\perp^2\boldsymbol{\Delta}_\perp^2 - 2(\mathbf{p}_\perp\cdot\boldsymbol{\Delta}_\perp)^2}{\boldsymbol{\Delta}_\perp^2}\right) + (1-x)\frac{\boldsymbol{\Delta}_\perp^2}{4}\right)\frac{T^\nu_{12}}{xM} - m\left(\left(\frac{\mathbf{p}_\perp^2\boldsymbol{\Delta}_\perp^2 - 2(\mathbf{p}_\perp\cdot\boldsymbol{\Delta}_\perp)^2}{\boldsymbol{\Delta}_\perp^2}\right) + (1-x)^2\frac{\boldsymbol{\Delta}_\perp^2}{4}\right)\frac{T^\nu_{22}}{x^2M^2}\right]d^2\mathbf{p}_\perp, \tag{30}$$

$$xE_{2T}^{\prime\nu(S)} = \int \frac{C_S^2 N_s^2}{4\pi^3}\left(-T_{11}^{\nu} + 2m(1-x)\frac{T_{12}^{\nu}}{xM} + 2\left(\frac{\mathbf{p}_\perp^2\boldsymbol{\Delta}_\perp^2 - (\mathbf{p}_\perp\cdot\boldsymbol{\Delta}_\perp)^2}{\boldsymbol{\Delta}_\perp^2}\right)\frac{T_{22}^{\nu}}{x^2M^2} - \left(\mathbf{p}_\perp^2 - (1-x)^2\frac{\boldsymbol{\Delta}_\perp^2}{4}\right)\frac{T_{22}^{\nu}}{x^2M^2}\right)$$
$$- 2\int \frac{C_S^2 N_s^2}{4\pi^3}\frac{M}{\boldsymbol{\Delta}_\perp^2}\left[\left(\left(\frac{\mathbf{p}_\perp^2\boldsymbol{\Delta}_\perp^2 - 2(\mathbf{p}_\perp\cdot\boldsymbol{\Delta}_\perp)^2}{\boldsymbol{\Delta}_\perp^2}\right) + (1-x)\frac{\boldsymbol{\Delta}_\perp^2}{4}\right)\frac{T_{12}^{\nu}}{xM} - m\left(\left(\frac{\mathbf{p}_\perp^2\boldsymbol{\Delta}_\perp^2 - 2(\mathbf{p}_\perp\cdot\boldsymbol{\Delta}_\perp)^2}{\boldsymbol{\Delta}_\perp^2}\right)\right.\right.$$
$$\left.\left. + (1-x)^2\frac{\boldsymbol{\Delta}_\perp^2}{4}\right)\frac{T_{22}^{\nu}}{x^2M^2}\right] d^2\mathbf{p}_\perp, \tag{31}$$

$$xE_{2T}^{\nu(A)} = \int \frac{C_A^2}{4\pi^3}\left(\frac{1}{3}|N_0^{\nu}|^2 + \frac{2}{3}|N_1^{\nu}|^2\right)\left(-T_{11}^{\nu} + 2m(1-x)\frac{T_{12}^{\nu}}{xM} + 2\left(\frac{\mathbf{p}_\perp^2\boldsymbol{\Delta}_\perp^2 - (\mathbf{p}_\perp\cdot\boldsymbol{\Delta}_\perp)^2}{\boldsymbol{\Delta}_\perp^2}\right)\frac{T_{22}^{\nu}}{x^2M^2}\right.$$
$$\left. - \left(\mathbf{p}_\perp^2 - (1-x)^2\frac{\boldsymbol{\Delta}_\perp^2}{4}\right)\frac{T_{22}^{\nu}}{x^2M^2}\right) + 2\int \frac{C_A^2}{4\pi^3}\left(\frac{1}{3}|N_0^{\nu}|^2\right)\frac{M}{\boldsymbol{\Delta}_\perp^2}\left[\left(\left(\frac{\mathbf{p}_\perp^2\boldsymbol{\Delta}_\perp^2 - 2(\mathbf{p}_\perp\cdot\boldsymbol{\Delta}_\perp)^2}{\boldsymbol{\Delta}_\perp^2}\right) + (1-x)\frac{\boldsymbol{\Delta}_\perp^2}{4}\right)\frac{T_{12}^{\nu}}{xM}\right.$$
$$\left. - m\left(\left(\frac{\mathbf{p}_\perp^2\boldsymbol{\Delta}_\perp^2 - 2(\mathbf{p}_\perp\cdot\boldsymbol{\Delta}_\perp)^2}{\boldsymbol{\Delta}_\perp^2}\right) + (1-x)^2\frac{\boldsymbol{\Delta}_\perp^2}{4}\right)\frac{T_{22}^{\nu}}{x^2M^2}\right] d^2\mathbf{p}_\perp. \tag{32}$$

It should be noted that GPDs xE_{2T}^{ν}, xH_{2T}^{ν}, and $x\tilde{H}_{2T}^{\nu}$ concerned with matrix structure γ^j and $x\tilde{E}_{2T}^{\prime\nu}$ concerning the matrix structure $\gamma^j\gamma_5$ were found to vanish in our calculation. This result is in line with the basis light-front quantization (BLFQ) findings [148]. Also, the lattice QCD computation of twist-3 chiral-even axial-vector GPD $x\tilde{E}_{2T}^{\prime\nu}$ comes out to be 0, which is in sync with our calculations [149].

V. RELATION WITH TWIST-3 GTMDS

Understanding the GTMD correlator structure and its parametrization equations is necessary to ascertain the relationship between GPDs and GTMDs. The GPD correlator for zero skewness $F^{\nu[\Gamma]}_{[\Lambda^{N_i}\Lambda^{N_f}]}(x,\Delta_\perp^2)$ can be expressed in terms of the fully unintegrated quark-quark GTMD correlator $W^{\nu[\Gamma]}_{[\Lambda^{N_i}\Lambda^{N_f}]}(x,\mathbf{p}_\perp^2,\Delta_\perp^2,\mathbf{p}_\perp\cdot\Delta_\perp)$ as [147]

$$F^{\nu[\Gamma]}_{[\Lambda^{N_i}\Lambda^{N_f}]}(x,\boldsymbol{\Delta}_\perp^2) = \int d^2\mathbf{p}_\perp W^{\nu[\Gamma]}_{[\Lambda^{N_i}\Lambda^{N_f}]}(x,\mathbf{p}_\perp^2,\boldsymbol{\Delta}_\perp^2,\mathbf{p}_\perp\cdot\boldsymbol{\Delta}_\perp). \tag{33}$$

According to Ref. [147], the quark GTMDs can be presented for different Dirac matrix structure values $\Gamma = \gamma^j$ and $\gamma^j\gamma_5$ as

$$W^{[\gamma^j]}_{[\Lambda^{N_i}\Lambda^{N_f}]} = \frac{1}{2P^+}\bar{u}(P^f,\Lambda^{N_f})\left[\frac{p_\perp^j}{M}F_{2,1} + \frac{\Delta_\perp^j}{M}F_{2,2} + \frac{Mi\sigma^{j+}}{P^+}F_{2,3} + \frac{p_\perp^j i\sigma^{\rho+}p_\perp^\rho}{MP^+}F_{2,4} + \frac{\Delta_\perp^j i\sigma^{\rho+}p_\perp^\rho}{MP^+}F_{2,5} + \frac{\Delta_\perp^j i\sigma^{\rho+}\Delta_\perp^\rho}{MP^+}F_{2,6}\right.$$
$$\left. + \frac{p_\perp^i i\sigma^{ij}}{M}F_{2,7} + \frac{\Delta_\perp^i i\sigma^{ij}}{M}F_{2,8}\right]u(P^i,\Lambda^{N_i}), \tag{34}$$

$$W^{[\gamma^j\gamma_5]}_{[\Lambda^{N_i}\Lambda^{N_f}]} = \frac{1}{2P^+}\bar{u}(P^f,\Lambda^{N_f})\left[-\frac{i\varepsilon_\perp^{ij}p_\perp^i}{M}G_{2,1} - \frac{i\varepsilon_\perp^{ij}\Delta_\perp^i}{M}G_{2,2} + \frac{Mi\sigma^{j+}\gamma_5}{P^+}G_{2,3} + \frac{p_\perp^j i\sigma^{\rho+}\gamma_5 p_\perp^\rho}{MP^+}G_{2,4} + \frac{\Delta_\perp^j i\sigma^{\rho+}\gamma_5 p_\perp^\rho}{MP^+}G_{2,5}\right.$$
$$\left. + \frac{\Delta_\perp^j i\sigma^{\rho+}\gamma_5\Delta_\perp^\rho}{MP^+}G_{2,6} + \frac{p_\perp^j i\sigma^{+-}\gamma_5}{M}G_{2,7} + \frac{\Delta_\perp^j i\sigma^{+-}\gamma_5}{M}G_{2,8}\right]u(P^i,\Lambda^{N_i}). \tag{35}$$

On solving the twist-3 GTMD parametrization parallel to the Eqs. (14) to (17), we get the following relations for Dirac matrix structure γ^j:

$$\frac{iP^+}{\boldsymbol{\Delta}_\perp^2}(\Delta_y(W^{\nu[\gamma^1]}_{[++]} - W^{\nu[\gamma^1]}_{[--]}) - \Delta_x(W^{\nu[\gamma^2]}_{[++]} - W^{\nu[\gamma^2]}_{[--]})) = 2\left[\frac{\mathbf{p}_\perp\cdot\boldsymbol{\Delta}_\perp}{\boldsymbol{\Delta}_\perp^2}F_{2,7} + F_{2,8}\right], \tag{36}$$

$$\frac{iP^+}{2M\boldsymbol{\Delta}_\perp^2}((\Delta_x + i\Delta_y)(\Delta_y W^{\nu[\gamma^1]}_{[-+]} - \Delta_x W^{\nu[\gamma^2]}_{[-+]}) = \left[-F_{2,3} + (\Delta_x - i\Delta_y)(\Delta_y W^{\nu[\gamma^1]}_{[+-]} - \Delta_x W^{\nu[\gamma^2]}_{[+-]})) + \frac{(\mathbf{p}_\perp\cdot\boldsymbol{\Delta}_\perp)^2 - \mathbf{p}_\perp^2\boldsymbol{\Delta}_\perp^2}{M^2\boldsymbol{\Delta}_\perp^2}F_{2,4}\right], \tag{37}$$

$$MP^+\left(\left(W^{\nu[\gamma^1]}_{[-+]}-W^{\nu[\gamma^1]}_{[+-]}\right)+i\left(W^{\nu[\gamma^2]}_{[-+]}+W^{\nu[\gamma^2]}_{[+-]}\right)\right)=[(\mathbf{p}_\perp\cdot\boldsymbol{\Delta}_\perp)F_{2,1}+\boldsymbol{\Delta}_\perp^2F_{2,2}-4M^2F_{2,3}-\mathbf{p}_\perp^2F_{2,4}-2(\mathbf{p}_\perp\cdot\boldsymbol{\Delta}_\perp)F_{2,5}-2\boldsymbol{\Delta}_\perp^2F_{2,6}], \tag{38}$$

$$P^+\left(\Delta_x\left(W^{\nu[\gamma^1]}_{[++]}+W^{\nu[\gamma^1]}_{[--]}\right)+\Delta_y\left(W^{\nu[\gamma^2]}_{[++]}+W^{\nu[\gamma^2]}_{[--]}\right)\right)=2[(\mathbf{p}_\perp\cdot\boldsymbol{\Delta}_\perp)F_{2,1}+\boldsymbol{\Delta}_\perp^2F_{2,2}]. \tag{39}$$

Similarly, from Eqs. (18) to (21) for the Dirac matrix structure $\Gamma=\gamma^j\gamma_5$ we get

$$\frac{P^+}{\Delta_\perp^2}\left(\Delta_x\left(W^{\nu[\gamma^1\gamma_5]}_{[++]}-W^{\nu[\gamma^1\gamma_5]}_{[--]}\right)+\Delta_y\left(W^{\nu[\gamma^2\gamma_5]}_{[++]}-W^{\nu[\gamma^2\gamma_5]}_{[--]}\right)\right)=4\left[\frac{\mathbf{p}_\perp\cdot\boldsymbol{\Delta}_\perp}{\boldsymbol{\Delta}_\perp^2}G_{2,7}+G_{2,8}\right], \tag{40}$$

$$\frac{P^+}{2M\boldsymbol{\Delta}_\perp^2}\left((\Delta_x+i\Delta_y)\left(\Delta_xW^{\nu[\gamma^1\gamma_5]}_{[-+]}+\Delta_yW^{\nu[\gamma^2\gamma_5]}_{[-+]}\right)\right)=\left[G_{2,3}+\frac{\boldsymbol{\Delta}_\perp^2}{M^2}\left(\frac{(\mathbf{p}_\perp\cdot\boldsymbol{\Delta}_\perp)^2}{\boldsymbol{\Delta}_\perp^4}G_{2,4}+(\Delta_x-i\Delta_y)\left(\Delta_xW^{\nu[\gamma^1\gamma_5]}_{[+-]}\Delta_yW^{\nu[\gamma^2\gamma_5]}_{[+-]}\right)\right)+\frac{(\mathbf{p}_\perp\cdot\boldsymbol{\Delta}_\perp)}{\boldsymbol{\Delta}_\perp^2}G_{2,5}+G_{2,6}\right)\Bigg], \tag{41}$$

$$MP^+\left(\left(W^{\nu[\gamma^1\gamma_5]}_{[-+]}-W^{\nu[\gamma^1\gamma_5]}_{[+-]}\right)+i\left(W^{\nu[\gamma^2\gamma_5]}_{[-+]}-W^{\nu[\gamma^2\gamma_5]}_{[+-]}\right)\right)=[(\mathbf{p}_\perp\cdot\boldsymbol{\Delta}_\perp)G_{2,1}+\boldsymbol{\Delta}_\perp^2G_{2,2}-4M^2G_{2,3}+2\mathbf{p}_\perp^2G_{2,4}+2(\mathbf{p}_\perp\cdot\boldsymbol{\Delta}_\perp)G_{2,5}+2\boldsymbol{\Delta}_\perp^2G_{2,6}], \tag{42}$$

$$P^+\left(\Delta_y\left(W^{\nu[\gamma^1\gamma_5]}_{[++]}+W^{\nu[\gamma^1\gamma_5]}_{[--]}\right)-\Delta_x\left(W^{\nu[\gamma^2\gamma_5]}_{[++]}+W^{\nu[\gamma^2\gamma_5]}_{[--]}\right)\right)=2i[(\mathbf{p}_\perp\cdot\boldsymbol{\Delta}_\perp)G_{2,1}+\boldsymbol{\Delta}_\perp^2G_{2,2}]. \tag{43}$$

To obtain the GPD relations with GTMDs, we have compared Eqs. (14) to (21) with Eqs. (36) to (43) via the use of Eq. (33):

$$H_{2T}(x,\xi,t)=\int d^2\mathbf{p}_\perp\left[-F_{2,3}+\frac{(\mathbf{p}_\perp\cdot\boldsymbol{\Delta}_\perp)^2-\mathbf{p}_\perp^2\boldsymbol{\Delta}_\perp^2}{M^2\boldsymbol{\Delta}_\perp^2}F_{2,4}\right], \tag{44}$$

$$E_{2T}(x,\xi,t)=\int d^2\mathbf{p}_\perp\left[4\left(\frac{2(\mathbf{p}_\perp\cdot\boldsymbol{\Delta}_\perp)^2-\mathbf{p}_\perp^2\boldsymbol{\Delta}_\perp^2}{(\boldsymbol{\Delta}_\perp^2)^2}F_{2,4}+\frac{(\mathbf{p}_\perp\cdot\boldsymbol{\Delta}_\perp)}{\boldsymbol{\Delta}_\perp^2}F_{2,5}+F_{2,6}\right)-4\left(\frac{(\mathbf{p}_\perp\cdot\boldsymbol{\Delta}_\perp)^2}{\boldsymbol{\Delta}_\perp^2}F_{2,7}+(\mathbf{p}_\perp\cdot\boldsymbol{\Delta}_\perp)F_{2,8}\right)\right] \tag{45}$$

$$\tilde{H}_{2T}(x,\xi,t)=\int d^2\mathbf{p}_\perp\left[\left(\frac{(\mathbf{p}_\perp\cdot\boldsymbol{\Delta}_\perp)}{\boldsymbol{\Delta}_\perp^2}F_{2,1}+F_{2,2}\right)-2\left(\frac{2(\mathbf{p}_\perp\cdot\boldsymbol{\Delta}_\perp)^2-\mathbf{p}_\perp^2\boldsymbol{\Delta}_\perp^2}{(\boldsymbol{\Delta}_\perp^2)^2}F_{2,4}+\frac{\mathbf{p}_\perp\cdot\boldsymbol{\Delta}_\perp}{\boldsymbol{\Delta}_\perp^2}F_{2,5}+F_{2,6}\right)\right], \tag{46}$$

$$\tilde{E}_{2T}(x,\xi,t)=\int d^2\mathbf{p}_\perp\left[-2\left(\frac{(\mathbf{p}_\perp\cdot\boldsymbol{\Delta}_\perp)}{\boldsymbol{\Delta}_\perp^2}F_{2,7}+F_{2,8}\right)\right], \tag{47}$$

$$H'_{2T}(x,\xi,t)=\int d^2\mathbf{p}_\perp\left[G_{2,3}+\frac{\boldsymbol{\Delta}_\perp^2}{M^2}\left(\frac{(\mathbf{p}_\perp\cdot\boldsymbol{\Delta}_\perp)^2}{(\boldsymbol{\Delta}_\perp^2)^2}G_{2,4}+\frac{\mathbf{p}_\perp\cdot\boldsymbol{\Delta}_\perp}{\boldsymbol{\Delta}_\perp^2}G_{2,5}+G_{2,6}\right)\right] \tag{48}$$

$$E'_{2T}(x,\xi,t)=\int d^2\mathbf{p}_\perp\left[4\left(\frac{2(\mathbf{p}_\perp\cdot\boldsymbol{\Delta}_\perp)^2-\mathbf{p}_\perp^2\boldsymbol{\Delta}_\perp^2}{(\boldsymbol{\Delta}_\perp^2)^2}G_{2,4}+\frac{\mathbf{p}_\perp\cdot\boldsymbol{\Delta}_\perp}{\boldsymbol{\Delta}_\perp^2}G_{2,5}+G_{2,6}\right)\right] \tag{49}$$

$$\tilde{H}'_{2T}(x,\xi,t)=\int d^2\mathbf{p}_\perp\left[\left(\frac{\mathbf{p}_\perp\cdot\boldsymbol{\Delta}_\perp}{\boldsymbol{\Delta}_\perp^2}G_{2,1}+G_{2,2}\right)-2\left(\frac{2(\mathbf{p}_\perp\cdot\boldsymbol{\Delta}_\perp)^2-\mathbf{p}_\perp^2\boldsymbol{\Delta}_\perp^2}{(\boldsymbol{\Delta}_\perp^2)^2}G_{2,4}+\frac{\mathbf{p}_\perp\cdot\boldsymbol{\Delta}_\perp}{\boldsymbol{\Delta}_\perp^2}G_{2,5}+G_{2,6}\right)\right], \tag{50}$$

$$\tilde{E}'_{2T}(x,\xi,t)=\int d^2\mathbf{p}_\perp\left[4\left(\frac{\mathbf{p}_\perp\cdot\boldsymbol{\Delta}_\perp}{\boldsymbol{\Delta}_\perp^2}G_{2,7}+G_{2,8}\right)\right]. \tag{51}$$

The twist-3 GPD-GTMD relations mentioned above have been satisfied by our calculations, similar to those that have been suggested in Ref. [147]. Contrary to that, in our exploration, we find that the relation given in Eqs. (45) and (51) is not followed. In the Eq. (45) relation, the GTMDs $F_{2,7}$ and $F_{2,8}$ appear whose contribution was found to be negligible while for the relation given in Eq. (51) a factor of 2 gets multiplied to the right-hand side.

VI. RELATION WITH TWIST-3 TMDS

By the application of zero momentum transfer limit on GTMDs $G_{2,3}$ and $G_{2,4}$, we can get the twist-3 TMDs $g'_T(x,\mathbf{p}_\perp^2)$ and $g_T^\perp(x,\mathbf{p}_\perp^2)$ sequentially. So, for $\boldsymbol{\Delta}_\perp = 0$ Eq. (48) is reduced to the following relation:

$$\begin{aligned} H'_{2T}(x,0,0) &= \int d^2\mathbf{p}_\perp \left[G^e_{2,3}(x,0,\mathbf{p}_\perp^2,0,0) \right. \\ &\quad \left. + \frac{\mathbf{p}_\perp^2}{2M^2} G^e_{2,4}(x,0,\mathbf{p}_\perp^2,0,0) \right] \\ &= \int d^2\mathbf{p}_\perp \left[g'_T(x,\mathbf{p}_\perp^2) + \frac{\mathbf{p}_\perp^2}{2M^2} g_T^\perp(x,\mathbf{p}_\perp^2) \right]. \end{aligned} \quad (52)$$

This relation can also be written as $g_T(x) = \lim_{\Delta\to 0} H'_{2T}(x,0,-t)$, where $g_T(x)$ is the PDF obtained from the concerned TMD and has also been verified for BLFQ in Ref. [148].

VII. DISCUSSION

This section presents the numerical results for twist-3 chiral-even GPDs of the proton in the LFQDM, focusing on the Dirac matrix structures γ^j and $\gamma^j\gamma_5$ at zero skewness. The discussion encompasses the twist-3 chiral-even GPDs, the twist-3 IPDPDFs, and the twist-3 FFs in the following subsections.

A. GPDs

Twist-3 chiral-even GPDs have been analyzed using both 2D and 3D plots. The 2D plots illustrate the variation of GPDs with respect to one variable while keeping the other variable fixed. In contrast, the 3D plots depict simultaneous changes in GPDs concerning the variables x and $\Delta_\perp$. The twist-3 chiral-even GPD $x\tilde{E}^\nu_{2T}$, concerning the matrix structure γ^j, has been plotted against x and $\Delta_\perp$ for the active u and d quarks in Fig. 3. The peaks of $x\tilde{E}^\nu_{2T}$ for active u and d quarks were found to exist in the low momentum transfer region, due to the occurrence of $\Delta_\perp$ in the denominator of Eqs. (25) and (26). This feature of the GPD matches the findings in Ref. [148]. The maxima of the plots for active u and d quarks were found around $x = 0.3$, suggesting the equal distribution of longitudinal momentum fraction x among each of the three valence quarks of the proton. This GPD comprises only S wave ($L_z = 0$). It was observed that the T_{11} term corresponds to the parallel spins of the active quark, and the parent proton contributes negatively, while for the antiparallel alignment, the T_{22} term contributes both negatively and positively to the distribution.

Now we refer to the GPDs connected with the matrix structure $\gamma^j\gamma_5$, which are xH'^ν_{2T}, $x\tilde{H}'^\nu_{2T}$, and xE'^ν_{2T}. These GPDs have been plotted in Fig. 3 for both the possible flavors of struck quark. Observations indicate that the GPD xH'^ν_{2T} peaks at lower values of $\Delta_\perp$, and when switching the active quark flavor from u to d, the peak of the distribution shifts slightly toward higher x. This GPD contains S-wave states from the T_{11} term, a P-wave state (with $L_z = 1$) from the T_{12} term, and a D-wave state (with $L_z = 2$) from the T_{22} term. From Eqs. (27) and (28), it is evident that the S-wave and P-wave contribute positively, while the D-wave contributes negatively to the distribution. The GPD $x\tilde{H}'^\nu_{2T}$ is plotted in Figs. 3(e) and 3(f) for the u and d quarks, respectively. Similar to xH'^ν_{2T}, this GPD also shows maxima at low values of x and $\Delta_\perp$. Notably, the sign of the amplitude for the active u quark distribution is positive, whereas for the active d quark distribution, it is negative. From Eqs. (29) and (30), it can be seen that $x\tilde{H}'^\nu_{2T}$ consists of a P-wave state from the T_{12} term and a D-wave state from the T_{22} term, both of which contribute oppositely to the GPD. Finally, the GPD xE'^ν_{2T} is represented in Figs. 3(g) and 3(h) for both active quark flavors ν. The plots reveal significant similarities between $x\tilde{E}^\nu_{2T}$ and $x\tilde{H}'^\nu_{2T}$. From the overlap form of this GPD, it is observed that this GPD consists of other axial-vector GPDs as well. Apart from the S-wave, which only makes a negative contribution to the GPD, the P-wave and D-waves make both positive and negative contributions.

To gain a better understanding of twist-3 chiral-even GPDs $x\tilde{E}^\nu_{2T}$, xH'^ν_{2T}, $x\tilde{H}'^\nu_{2T}$, and xE'^ν_{2T}, we have investigated their behavior in relation to the longitudinal momentum fraction x at various fixed transverse momentum transfer values $\Delta_\perp$ for both active quark flavors ($\nu = u, d$). The key observations from Fig. 4 include that $x\tilde{E}^\nu_{2T}$ increases as the longitudinal momentum fraction x increases, and after attaining a maximum value, it decreases for higher values of x at different values of $\Delta_\perp$. The maxima of each GPD shifts toward higher x as the transverse momentum transfer $\Delta_\perp$ is increased. In all GPDs, at very high values of x, the curves corresponding to the different values of $\Delta_\perp$ merge with each other. This suggests that at very high x, the momentum transfer $\Delta_\perp$ becomes ineffective for both u and d active quark flavors. We also plot the GPDs in relation to $\Delta_\perp$ for different values of x for both active quark flavors u and d. From Fig. 5, it is apparent that all the GPDs follow a similar trend. As x increases to high values, the peak of the distributions becomes broader, suggesting that the contributions to higher $\Delta_\perp$ come from high values of x. Conversely, for low values of x, such as 0.25, the plots

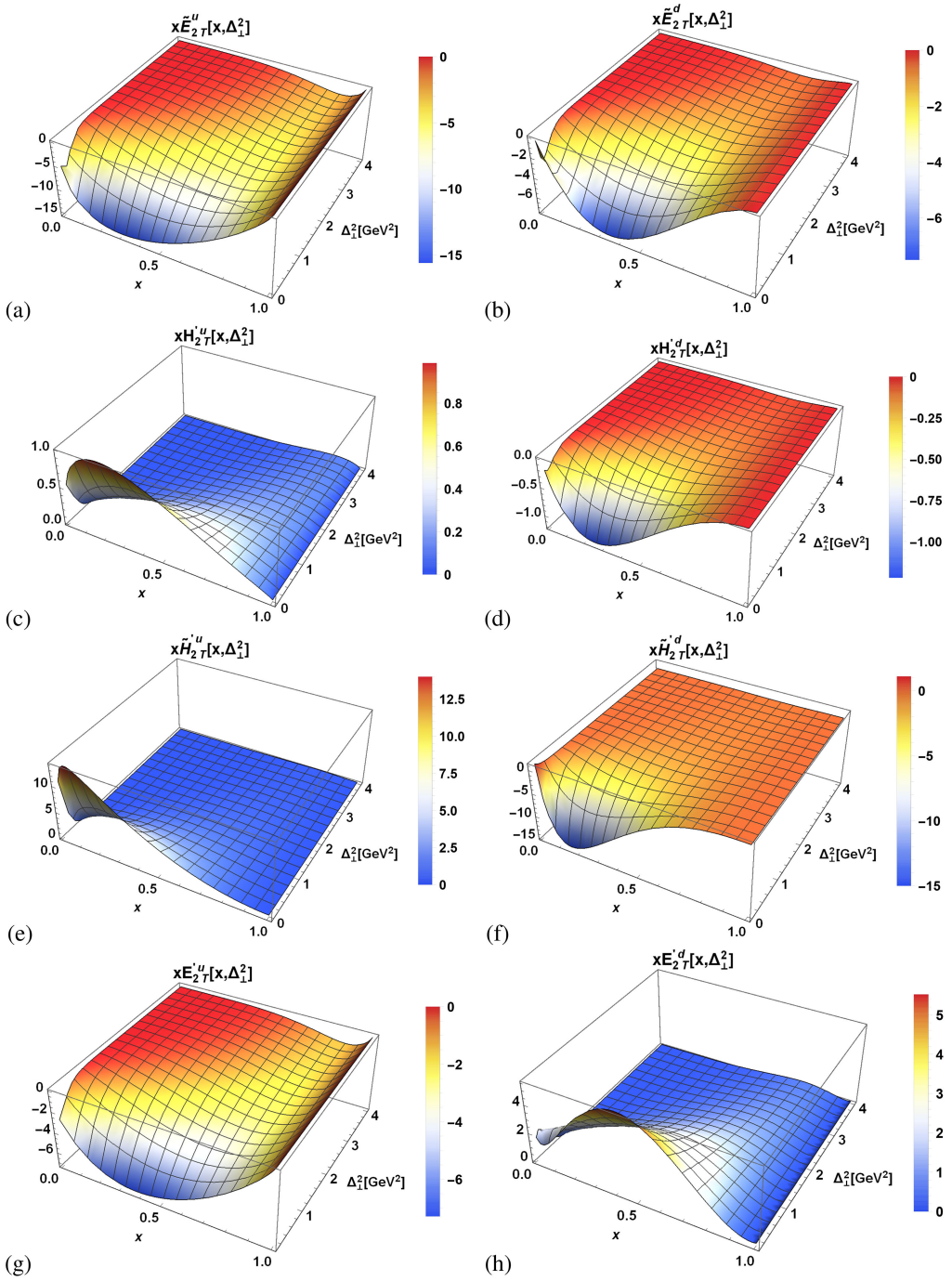

FIG. 3. Plots of the chiral-even twist-3 GPDs $x\tilde{E}^{\nu}_{2T}$, xH'^{ν}_{2T}, $x\tilde{H}'^{\nu}_{2T}$, and xE'^{ν}_{2T} are shown against x and $\boldsymbol{\Delta}^2_\perp$. Figures (a), (c), (e), and (g) represent the active u quark distributions whereas (b), (d), (f), and (h) represent active d quark distributions.

become sharp, and negligible contributions are seen for high values of $\Delta_\perp$.

B. Impact parameter dependent parton distributions

A distinct viewpoint on the spatial parton distribution within hadrons is offered by the impact parameter space GPDs, also known as IPDPDFs [150]. These distributions offer an additional viewpoint on the spatial distribution of partons within hadrons by describing the probability amplitude of locating a parton at a certain transverse distance $\mathbf{b}_\perp$ from the hadron center. The Fourier transform is carried out in $\boldsymbol{\Delta}_\perp$ to produce IPDPDFs as [124]

$$\mathcal{X}^{\nu}(x,\mathbf{b}_\perp)=\frac{1}{(2\pi)^2}\int d^2\boldsymbol{\Delta}_\perp e^{-ib_\perp\cdot\boldsymbol{\Delta}_\perp}X^{\nu}(x,\boldsymbol{\Delta}^2_\perp). \quad (53)$$

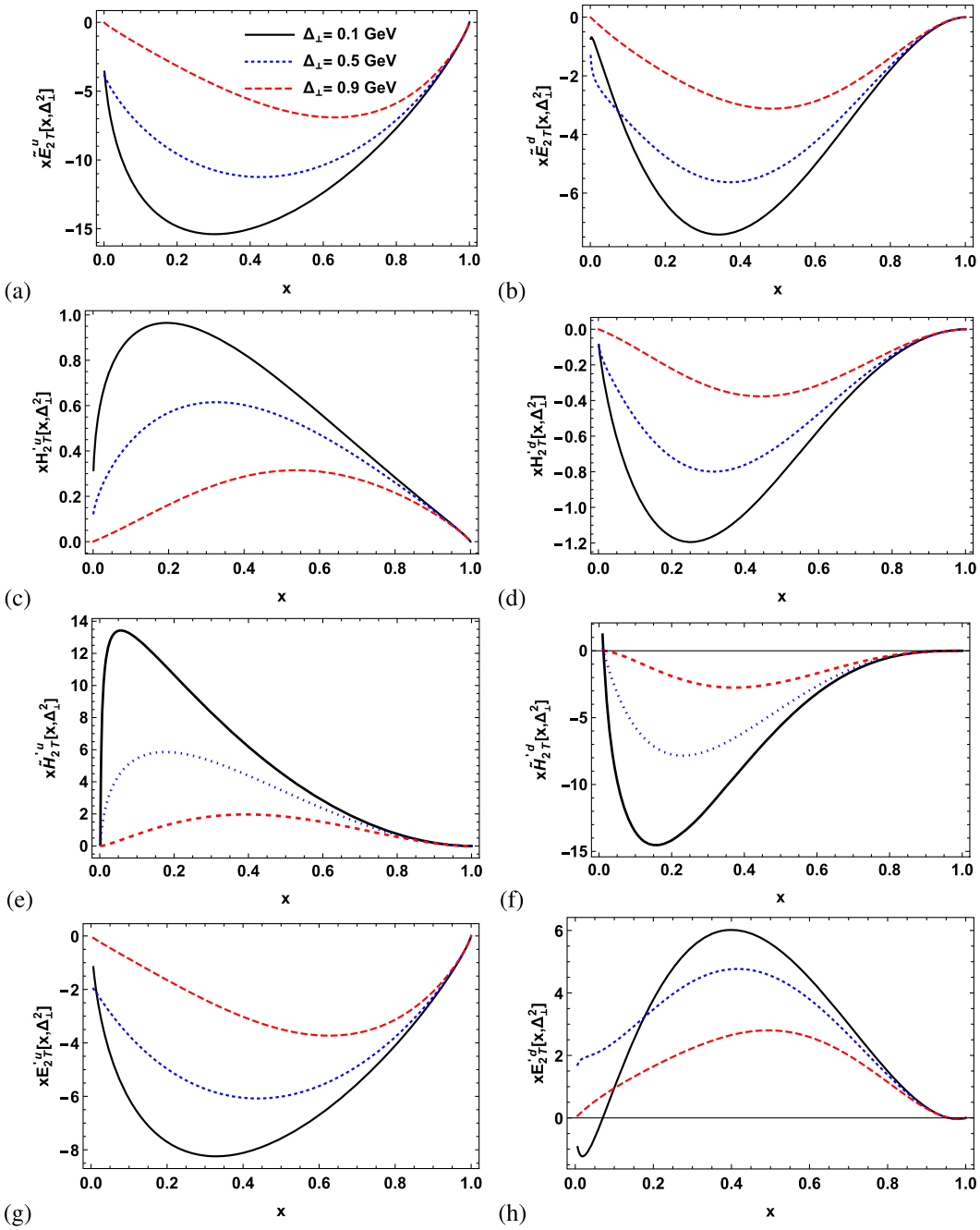

FIG. 4. The chiral-even twist-3 GPDs $x\tilde{E}^{\nu}_{2T}$, xH'^{ν}_{2T}, $x\tilde{H}'^{\nu}_{2T}$, and xE'^{ν}_{2T} plotted with respect to x at various fixed values of $\mathbf{\Delta}_\perp$. Figures (a), (c), (e), and (g) represent the active u quark distributions whereas (b), (d), (f), and (h) represent active d quark distributions.

Here, $X^{\nu}(x, \mathbf{\Delta}^2_\perp)$ and $\mathcal{X}^{\nu}(x, \mathbf{b}_\perp)$ denote the corresponding GPD and IPDPDF sequentially. We have plotted twist-3 IPDPDFs ($x\tilde{\mathcal{E}}^{\nu}_{2T}$, $x\mathcal{H}'^{\nu}_{2T}$, $x\tilde{\mathcal{H}}'^{\nu}_{2T}$, and $x\mathcal{E}'^{\nu}_{2T}$) in Fig. 6 for both the possibilities of the active quark flavor being u or d. IPDPDF $x\tilde{\mathcal{E}}^{\nu}_{2T}$ has been plotted in Figs. 6(a) and 6(b), which shows that $x\tilde{\mathcal{E}}^{\nu}_{2T}$ has a high probability of being concentrated toward the center of momentum (COM) line and as the longitudinal momentum fraction x is increased the peak of distribution for active u becomes more negative and approaches zero for higher values of $b_\perp$ while for active d quark distribution, the maximum peak is observed for the longitudinal momentum fraction being about 0.5. Plots in Figs. 6(c) and 6(d) show that the sign of the amplitude of the distribution reverses on the change of active quark flavor for the polarization configuration corresponding to IPDPD $x\mathcal{H}'^{\nu}_{2T}$. For active d quark, the distribution corresponding to $x\mathcal{H}'^{\nu}_{2T}$ is similar to that of $x\tilde{\mathcal{E}}^{\nu}_{2T}$, keeping magnitude aside. In Figs. 6(e) and 6(f), IPDPDF $x\tilde{\mathcal{H}}'^{\nu}_{2T}$

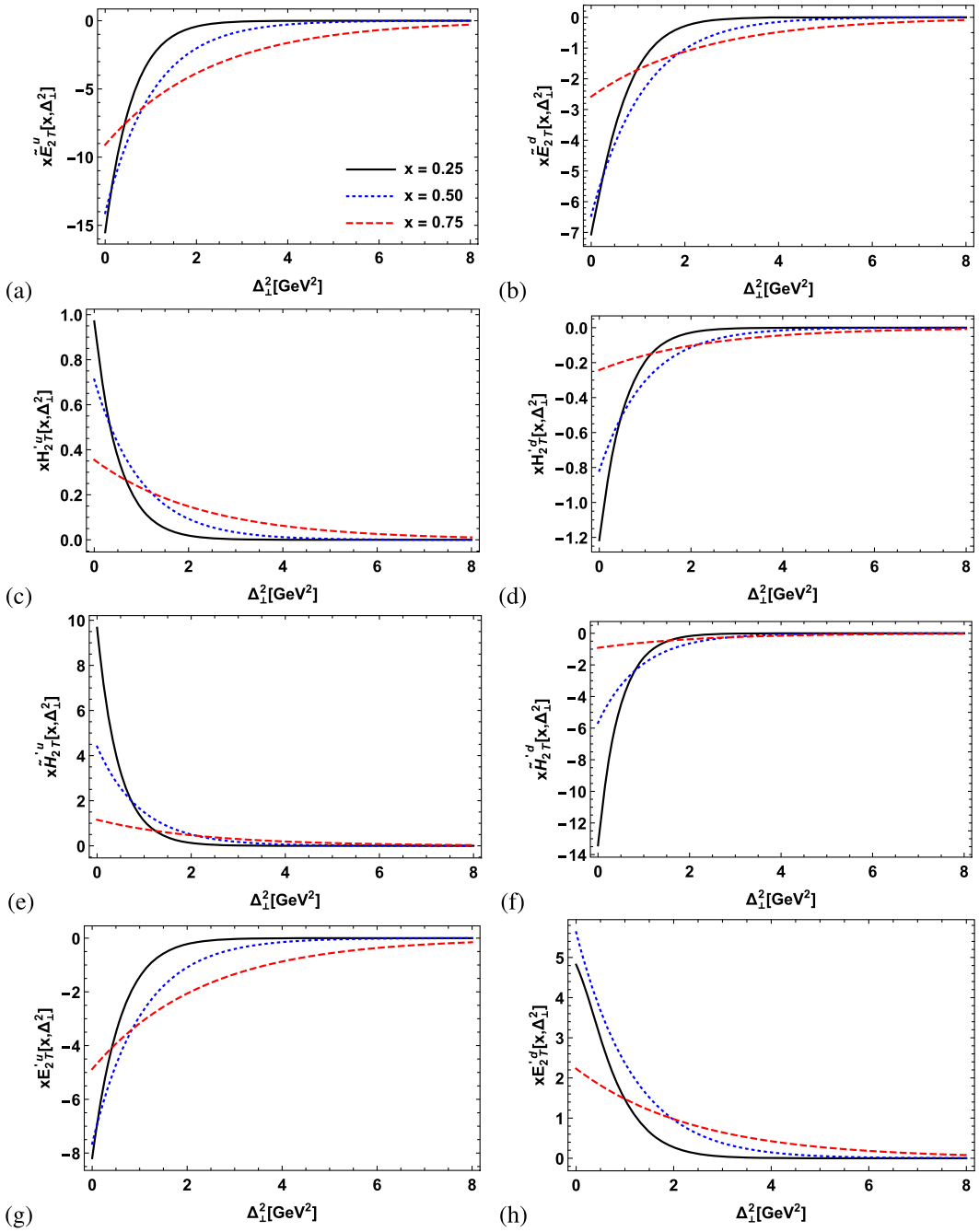

FIG. 5. The chiral-even twist-3 GPDs $x\tilde{E}^{\nu}_{2T}$, xH'^{ν}_{2T}, $x\tilde{H}'^{\nu}_{2T}$, and xE'^{ν}_{2T} plotted with respect to $\mathbf{\Delta}^2_\perp$ at various fixed values of x. Figures (a), (c), (e), and (g) represent the active u quark distributions whereas (b), (d), (f), and (h) represent active d quark distributions.

is plotted for each active quark flavor. While considering the behavior of distribution along the longitudinal momentum fraction x, plots of $x\tilde{\mathcal{H}}'^{\nu}_{2T}$ show the most distinct trend from the remaining distributions in a sense that the lines corresponding to different x are not tangled. Furthermore, it has been noted that when x decreases, the distribution's magnitude grows for both active quark flavors ($\nu = u, d$). For the IPDPDF $x\mathcal{E}'^{\nu}_{2T}$, the plots corresponding to this distribution are found to be remarkably similar in trend to those of $x\tilde{\mathcal{E}}^{\nu}_{2T}$, although they differ in amplitude. Another distinction is that the plots for $x\tilde{\mathcal{E}}^{\nu}_{2T}$ exhibit the same polarity for different flavors of the active quark, whereas $x\mathcal{E}'^{\nu}_{2T}$ does not. To provide a clearer understanding of the possibility of the active quark being near the COM, we have depicted the distributions using contour plots in Fig. 7, where GPDs are shown as functions of the transverse coordinates b_x and b_y. These plots allow us to visualize the spatial distribution of quarks within the hadron, giving us

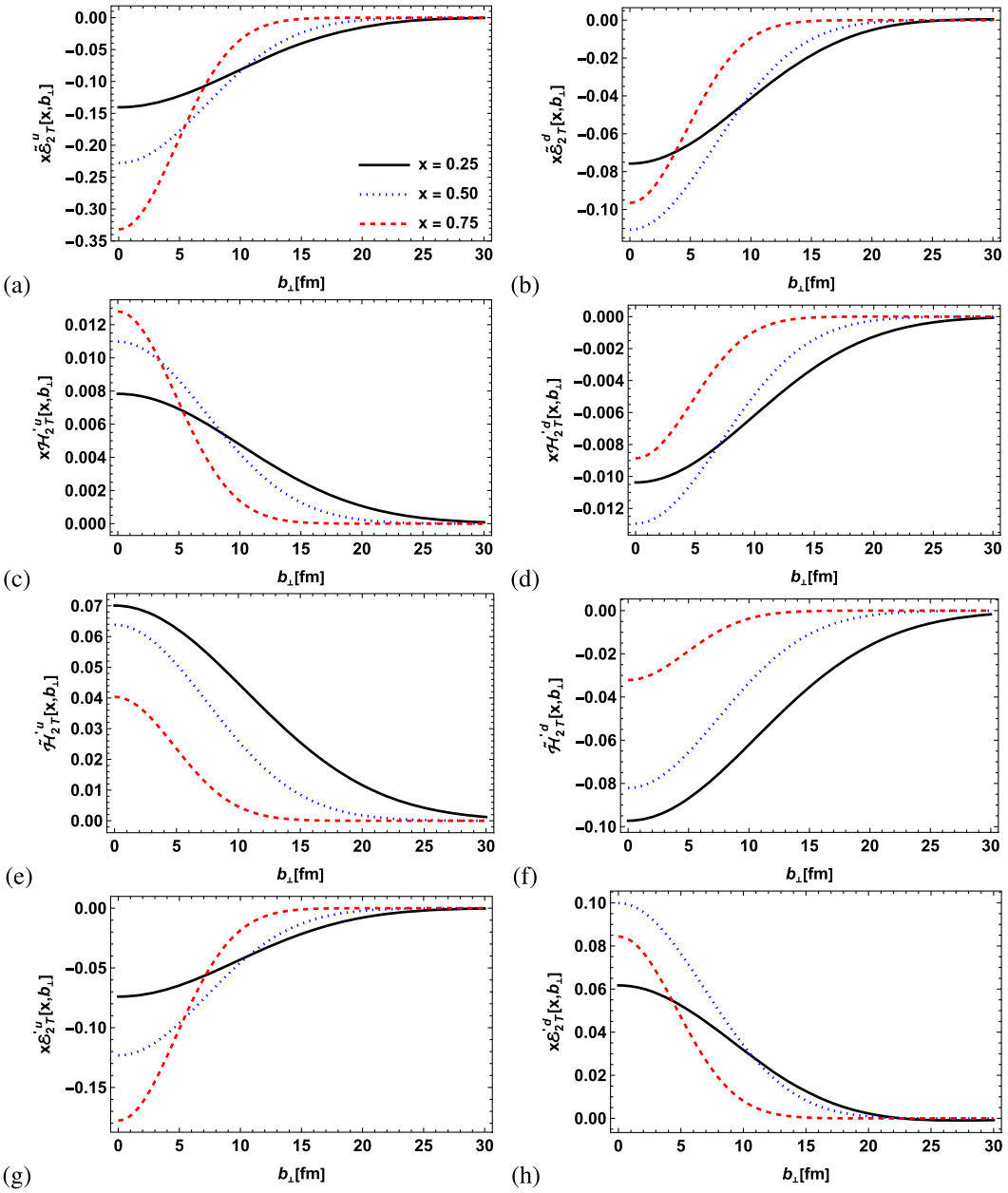

FIG. 6. The twist-3 IPDPDFs $x\tilde{\mathcal{E}}^{\nu}_{2T}$, $x\mathcal{H}'^{\nu}_{2T}$, $x\tilde{H}'^{\nu}_{2T}$, and $x\mathcal{E}'^{\nu}_{2T}$ plotted with respect to $\mathbf{b}_\perp$ at various fixed values of x. Figures (a), (c), (e), and (g) represent the active u quark distributions whereas (b), (d), (f), and (h) represent active d quark distributions.

insights into how the quark density varies in the transverse plane. Here the circular symmetry observed in Fig. 7 with respect to variables b_x and b_y arises because of the equal contribution of these variables to the GPD expressions. In certain scenarios, particularly when specific directions are emphasized in the definition of the distributions, for instance in spin densities, noncircular symmetry can appear when transverse directions are weighted differently [137].

C. Form factors

In Fig. 8, we have plotted the twist-3 FFs ($x\tilde{E}^{\nu}_{2T}$, xH'^{ν}_{2T}, $x\tilde{H}'^{\nu}_{2T}$, and xE'^{ν}_{2T}) obtained by integrating twist-3 chiral-even GPDs over the longitudnal momentum fraction x. At first glance, the magnitude of all the FF plots appears to exponentially approach zero when the transverse momentum transfer to the proton square $(\Delta^2_\perp)$ reaches higher values. This exponential trend underscores the strong suppression of quark distributions at higher transverse

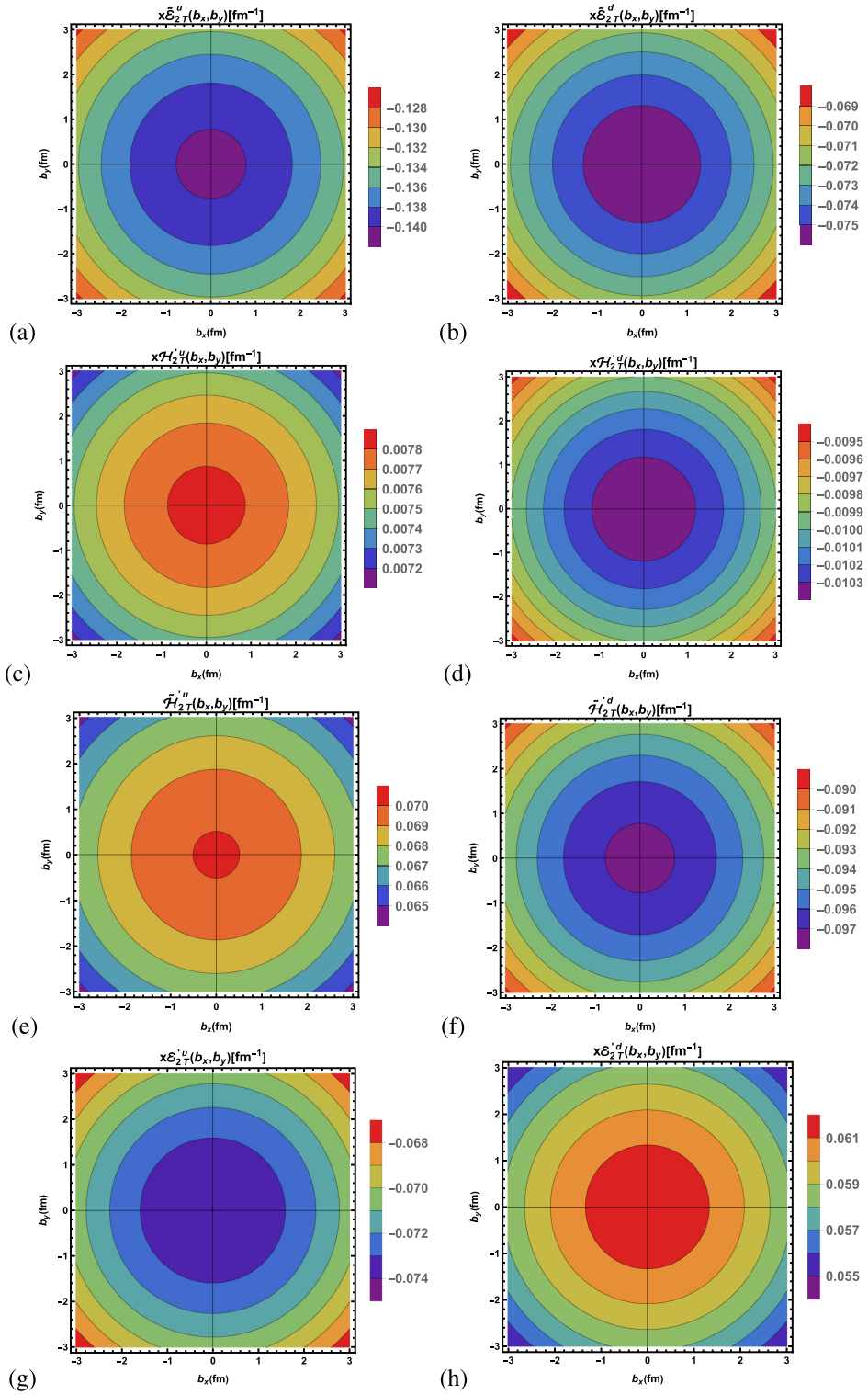

FIG. 7. The twist-3 IPDPDFs $x\tilde{\mathcal{E}}_{2T}^{\nu}$, $x\mathcal{H}_{2T}^{\prime\nu}$, $x\tilde{\mathcal{H}}_{2T}^{\prime\nu}$, and $x\mathcal{E}_{2T}^{\prime\nu}$ plotted with respect to b_x and b_y at various fixed values of $x = 0.25$. Figures (a), (c), (e), and (g) represent the active u quark distributions whereas (b), (d), (f), and (h) represent active d quark distributions.

momentum transfers, highlighting the intricate spatial configuration of the proton's internal structure.

In contrast to twist-2 FFs, which are well established and possess a robust probabilistic interpretation, the exploration and theoretical understanding of twist-3 FFs remain relatively underdeveloped. Our goal is to compare our findings with those obtained for lower-twist FFs, as discussed in Ref. [137]. However, it is important to note

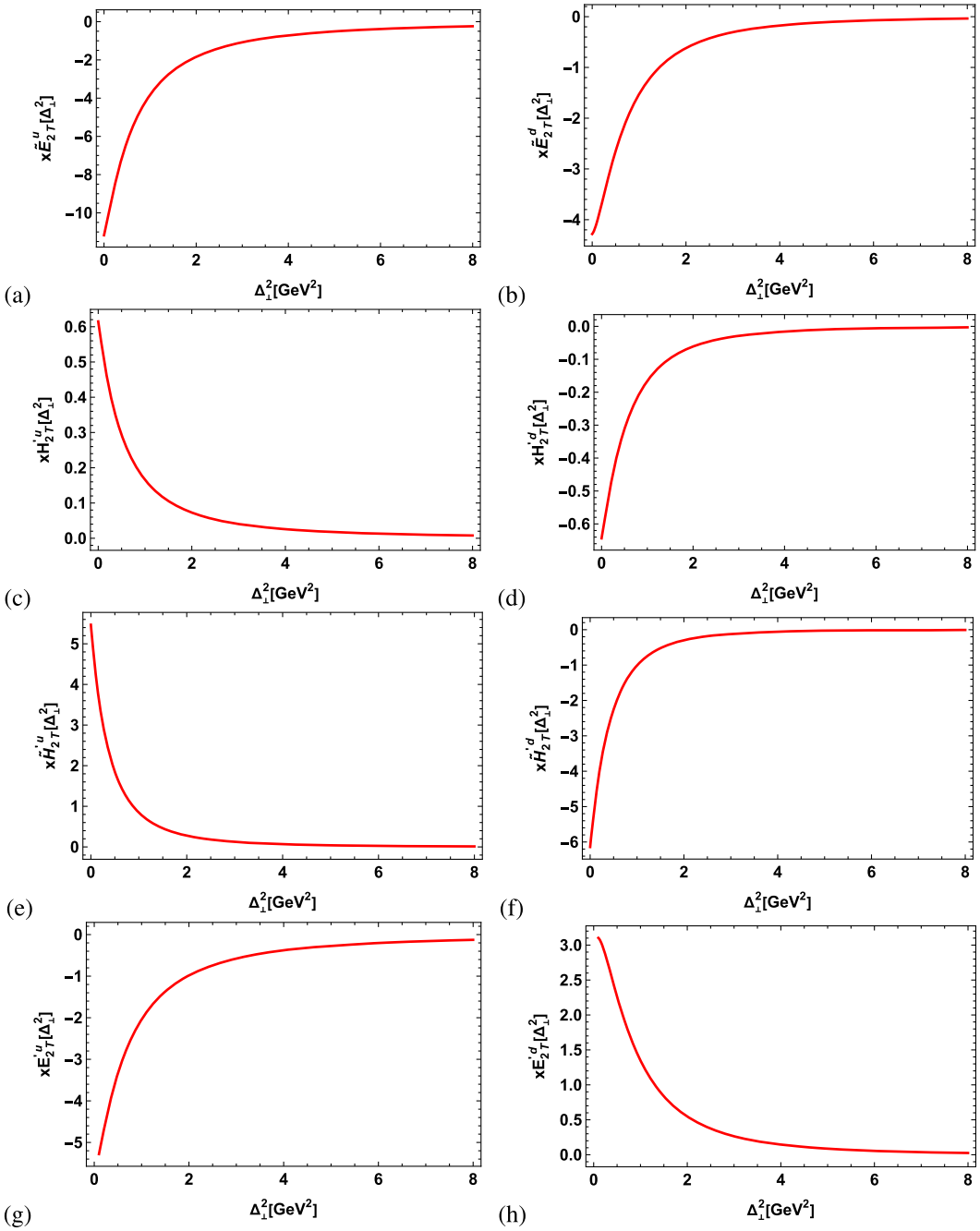

FIG. 8. The twist-3 FFs $x\tilde{E}^{\nu}_{2T}$, xH'^{ν}_{2T}, $x\tilde{H}'^{\nu}_{2T}$, and xE'^{ν}_{2T} plotted with respect to $\mathbf{\Delta}_\perp^2$. Figures (a), (c), (e), and (g) represent the active u quark distributions whereas (b), (d), (f), and (h) represent active d quark distributions.

that the chiral-even GPDs at twist-2 have different parametrization structures compared to those at twist-3, as highlighted in Ref. [147]. This structural difference complicates direct comparisons between twist-2 and twist-3 FFs, unlike the more straightforward relationship between twist-2 and twist-4 GPDs, where each lower-twist GPD has a higher-twist counterpart [147]. For completeness, we compare our twist-3 FF results with those of the leading-twist (twist-2) FFs in Fig. 9. For plotting purposes, we address the singularity at $x = 0$ by multiplying all FFs by x. To facilitate comparison, we plot the twist-2 FFs xE^{ν} (xH^{ν}) alongside all nonzero twist-3 FFs, including $x\tilde{E}^{\nu}_{2T}$, xE'^{ν}_{2T} (xH'^{ν}_{2T}, $x\tilde{H}'^{\nu}_{2T}$). As seen in Fig. 9, the twist-2 FFs xE^{ν} and xH^{ν} exhibit trends similar to those of the twist-3 FFs. Notably, both twist-2 and twist-3 FFs share the same polarity for the active u quark distributions. However, this is not the case for the active d quark distributions, where a negative sign has been introduced with some FFs to emphasize their differences.

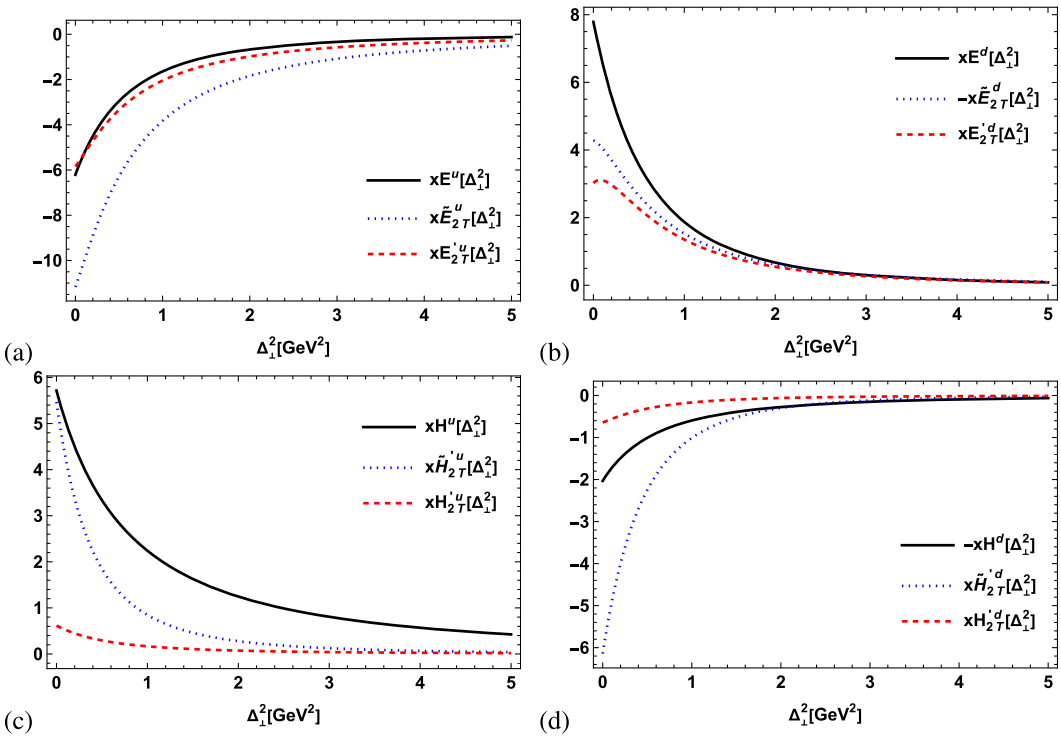

FIG. 9. FFs at twist-2 xE^ν (xH^ν) have been plotted with twist-3 FFs of $x\tilde{E}^\nu_{2T}$, xE'^ν_{2T} (xH'^ν_{2T}, $x\tilde{H}'^\nu_{2T}$) with respect to Δ^2. Figures (a) and (c) represent the active u quark distributions whereas (b) and (d) represent active d quark distributions.

VIII. CONCLUSION

In our study of twist-3 chiral-even GPDs within the LFQDM, we have derived the expressions for the concerned GPDs by solving the appropriate parametrization equations. Using the light-front wave functions (LFWFs) for both scalar and vector diquark configurations, we have obtained the GPDs for both possible cases of diquarks. Explicit equations were derived for the scenarios where the active quark flavor is either u or d. We have utilized the relationship between the GTMD correlator and the GPD correlator to establish the connection between twist-3 chiral-even GPDs and twist-3 GTMDs. Most of these relations are consistent with those presented in Ref. [147]. Some of our results are also in agreement with findings from the BLFQ approach [148] and the lattice QCD [149]. We have done a detailed discussion on twist-3 GPDs, IPDPDFs, and FFs by employing 2D and 3D plots to illustrate the variation of these expressions with respect to the kinematic variables, providing a comprehensive understanding of their behavior.

The discovery of exclusive reactions involving GPDs is about to enter a new era with the arrival of the Electron-Ion Collider (EIC) at Brookhaven National Laboratory. With its cutting-edge capabilities, the EIC is poised to deliver unprecedented precision in experimental data, enabling a thorough examination of the strong force and the refinement of existing GPD models. By enhancing lattice QCD calculations and developing sophisticated phenomenological models, we can better interpret the plethora of data from such advanced experiments. GPDs have already broadened our understanding of proton structure, and the precise data provided by these advanced tools will enable us to gain deeper insights into the complexities of the strong force and assess the limitations of current GPD models. Future theoretical works on GPDs, such as calculating nonzero skewness distributions with the inclusion of higher Fock states across different proton polarizations, will be crucial to support these experimental developments. In the future, it would be fascinating to explore model-independent calculations of these higher twist distributions, especially in the low-x regime.

ACKNOWLEDGMENTS

H. D. would like to thank the Science and Engineering Research Board, Anusandhan-National Research Foundation, Government of India under the scheme SERB-POWER Fellowship (Ref. No. SPF/2023/000116) for financial support.

[1] J. Gao, L. Harland-Lang, and J. Rojo, Phys. Rep. **742**, 1 (2018).
[2] G. Altarelli and G. G. Ross, Phys. Lett. B **212**, 391 (1988).
[3] M. Anselmino, A. Efremov, and E. Leader, Phys. Rep. **261**, 1 (1995); **281**, 399(E) (1997).
[4] R. D. Ball, S. Forte, and G. Ridolfi, Phys. Lett. B **378**, 255 (1996).
[5] S. D. Bass, Rev. Mod. Phys. **77**, 1257 (2005).
[6] G. Altarelli, R. D. Ball, S. Forte, and G. Ridolfi, Acta Phys. Pol. B **29**, 1145 (1998).
[7] F. Bissey, F. G. Cao, and A. I. Signal, Phys. Rev. D **73**, 094008 (2006).
[8] F. Wilczek, Central Eur. J. Phys. **10**, 1021 (2012).
[9] X. D. Ji, Phys. Rev. Lett. **74**, 1071 (1995).
[10] C. Lorcé, Eur. Phys. J. C **78**, 120 (2018).
[11] A. Metz, B. Pasquini, and S. Rodini, Phys. Rev. D **102**, 114042 (2020).
[12] R. Wang, J. Evslin, and X. Chen, Eur. Phys. J. C **80**, 507 (2020).
[13] P. L. Anthony *et al.* (E142 Collaboration), Phys. Rev. Lett. **71**, 959 (1993).
[14] K. Abe *et al.* (E143 Collaboration), Phys. Rev. D **58**, 112003 (1998).
[15] K. Abe *et al.* (E154 Collaboration), Phys. Rev. Lett. **79**, 26 (1997).
[16] P. L. Anthony *et al.* (E155 Collaboration), Phys. Lett. B **458**, 529 (1999).
[17] P. L. Anthony *et al.* (E155 Collaboration), Phys. Lett. B **493**, 19 (2000).
[18] P. L. Anthony *et al.* (E155 Collaboration), Phys. Lett. B **553**, 18 (2003).
[19] B. Adeva *et al.* (Spin Muon (SMC) Collaboration), Phys. Lett. B **412**, 414 (1997).
[20] D. Adams *et al.* (Spin Muon (SMC) Collaboration), Phys. Rev. D **56**, 5330 (1997).
[21] B. Adeva *et al.* (Spin Muon Collaboration), Phys. Rev. D **58**, 112001 (1998).
[22] M. G. Alekseev *et al.* (COMPASS Collaboration), Phys. Lett. B **690**, 466 (2010).
[23] C. Adolph *et al.* (COMPASS Collaboration), Phys. Lett. B **753**, 18 (2016).
[24] C. Adolph *et al.* (COMPASS Collaboration), Phys. Lett. B **769**, 34 (2017).
[25] A. Airapetian *et al.* (HERMES Collaboration), Phys. Lett. B **442**, 484 (1998).
[26] A. Airapetian *et al.* (HERMES Collaboration), Phys. Rev. D **75**, 012007 (2007).
[27] A. Airapetian *et al.* (HERMES Collaboration), Eur. Phys. J. C **72**, 1921 (2012).
[28] R. Fatemi *et al.* (CLAS Collaboration), Phys. Rev. Lett. **91**, 222002 (2003).
[29] K. Kramer, D. S. Armstrong, T. D. Averett, W. Bertozzi, S. Binet, C. Butuceanu, A. Camsonne, G. D. Cates, J. P. Chen, S. Choi *et al.*, Phys. Rev. Lett. **95**, 142002 (2005).
[30] K. V. Dharmawardane *et al.* (CLAS Collaboration), Phys. Lett. B **641**, 11 (2006).
[31] Y. Prok *et al.* (CLAS Collaboration), Phys. Rev. C **90**, 025212 (2014).
[32] A. Deur, Y. Prok, V. Burkert, D. Crabb, F. X. Girod, K. A. Griffioen, N. Guler, S. E. Kuhn, and N. Kvaltine, Phys. Rev. D **90**, 012009 (2014).
[33] J. C. Collins and D. E. Soper, Nucl. Phys. **B193**, 381 (1981); **B213**, 545(E) (1983).
[34] X. D. Ji, J. P. Ma, and F. Yuan, Phys. Rev. D **71**, 034005 (2005).
[35] H. L. Lai, M. Guzzi, J. Huston, Z. Li, P. M. Nadolsky, J. Pumplin, and C. P. Yuan, Phys. Rev. D **82**, 074024 (2010).
[36] J. Chay and C. Kim, J. High Energy Phys. 09 (2013) 126.
[37] M. Gluck, E. Reya, and A. Vogt, Z. Phys. C **67**, 433 (1995).
[38] J. C. Collins and D. E. Soper, Nucl. Phys. **B194**, 445 (1982).
[39] W. Chen, F. Feng, and Y. Jia, arXiv:2406.19994.
[40] J. D. Bjorken, Phys. Rev. **179**, 1547 (1969).
[41] R. Wang, C. Han, and X. Chen, arXiv:2407.16122.
[42] K. G. Wilson, Phys. Rev. **179**, 1499 (1969).
[43] R. A. Brandt and G. Preparata, Nucl. Phys. **B27**, 541 (1971).
[44] N. H. Christ, B. Hasslacher, and A. H. Mueller, Phys. Rev. D **6**, 3543 (1972).
[45] D. W. Sivers, Phys. Rev. D **41**, 83 (1990).
[46] D. Boer and P. J. Mulders, Phys. Rev. D **57**, 5780 (1998).
[47] S. J. Brodsky, B. Pasquini, B. W. Xiao, and F. Yuan, Phys. Lett. B **687**, 327 (2010).
[48] J. C. Collins, S. F. Heppelmann, and G. A. Ladinsky, Nucl. Phys. **B420**, 565 (1994).
[49] D. Boer, R. Jakob, and P. J. Mulders, Nucl. Phys. **B504**, 345 (1997).
[50] D. Boer, Phys. Rev. D **60**, 014012 (1999).
[51] A. Bacchetta, M. Boglione, A. Henneman, and P. J. Mulders, Phys. Rev. Lett. **85**, 712 (2000).
[52] S. Arnold, A. Metz, and M. Schlegel, Phys. Rev. D **79**, 034005 (2009).
[53] J. C. Collins, D. E. Soper, and G. F. Sterman, Nucl. Phys. **B250**, 199 (1985).
[54] P. J. Mulders and R. D. Tangerman, Nucl. Phys. **B461**, 197 (1996); **B484**, 538(E) (1997).
[55] A. Kotzinian, Nucl. Phys. **B441**, 234 (1995).
[56] A. V. Belitsky, X. Ji, and F. Yuan, Nucl. Phys. **B656**, 165 (2003).
[57] I. O. Cherednikov and N. G. Stefanis, Phys. Rev. D **77**, 094001 (2008).
[58] M. Burkardt, Phys. Rev. D **66**, 114005 (2002).
[59] P. V. Pobylitsa, arXiv:hep-ph/0301236.
[60] K. Goeke, A. Metz, and M. Schlegel, Phys. Lett. B **618**, 90 (2005).
[61] S. J. Brodsky and F. Yuan, Phys. Rev. D **74**, 094018 (2006).
[62] H. Avakian, S. J. Brodsky, A. Deur, and F. Yuan, Phys. Rev. Lett. **99**, 082001 (2007).
[63] G. A. Miller, Phys. Rev. C **76**, 065209 (2007).
[64] Ph. Hägler, B. U. Musch, J. W. Negele, and A. Schäfer, Europhys. Lett. **88**, 61001 (2009).
[65] R. N. Cahn, Phys. Lett. **78B**, 269 (1978).
[66] A. König and P. Kroll, Z. Phys. C **16**, 89 (1982).
[67] P. Chiappetta and M. Le Bellac, Z. Phys. C **32**, 521 (1986).

[68] A. V. Efremov, L. Mankiewicz, and N. A. Tornqvist, Phys. Lett. B **284**, 394 (1992).
[69] J. C. Collins, Nucl. Phys. **B396**, 161 (1993).
[70] J. C. Collins, Phys. Lett. B **536**, 43 (2002).
[71] A. Bacchetta, M. Diehl, K. Goeke, A. Metz, P. J. Mulders, and M. Schlegel, J. High Energy Phys. 02 (2007) 093.
[72] S. J. Brodsky, D. S. Hwang, and I. Schmidt, Phys. Lett. B **530**, 99 (2002).
[73] S. Falciano *et al.* (NA10 Collaboration), Z. Phys. C **31**, 513 (1986).
[74] J. S. Conway *et al.*, Phys. Rev. D **39**, 92 (1989).
[75] L. Y. Zhu *et al.* (FNAL-E866/NuSea Collaboration), Phys. Rev. Lett. **99**, 082301 (2007).
[76] M. Arneodo *et al.* (European Muon Collaboration), Z. Phys. C **34**, 277 (1987).
[77] A. Airapetian *et al.* (HERMES Collaboration), Phys. Rev. Lett. **84**, 4047 (2000).
[78] H. Avakian *et al.* (CLAS Collaboration), Phys. Rev. D **69**, 112004 (2004).
[79] A. Airapetian *et al.* (HERMES Collaboration), Phys. Rev. Lett. **94**, 012002 (2005).
[80] V. Y. Alexakhin *et al.* (COMPASS Collaboration), Phys. Rev. Lett. **94**, 202002 (2005).
[81] I. M. Gregor (HERMES Collaboration), Acta Phys. Pol. B **36**, 209 (2005).
[82] E. S. Ageev *et al.* (COMPASS Collaboration), Nucl. Phys. **B765**, 31 (2007).
[83] A. Airapetian *et al.* (HERMES Collaboration), Phys. Lett. B **622**, 14 (2005).
[84] A. Kotzinian (COMPASS Collaboration), arXiv:0705.2402.
[85] M. Diefenthaler, AIP Conf. Proc. **792**, 933 (2005).
[86] M. Osipenko *et al.* (CLAS Collaboration), Phys. Rev. D **80**, 032004 (2009).
[87] F. Giordano, R. Lamb (HERMES Collaboration), AIP Conf. Proc. **1149**, 423 (2009).
[88] A. Airapetian *et al.* (HERMES Collaboration), Phys. Lett. B **684**, 114 (2010).
[89] X. D. Ji, J. Phys. G **24**, 1181 (1998).
[90] D. Müller, D. Robaschik, B. Geyer, F.-M. Dittes, and J. Hořejši, Fortschr. Phys. **42**, 101 (1994).
[91] X. D. Ji, Phys. Rev. Lett. **78**, 610 (1997).
[92] A. V. Radyushkin, Phys. Lett. B **380**, 417 (1996).
[93] K. Goeke, M. V. Polyakov, and M. Vanderhaeghen, Prog. Part. Nucl. Phys. **47**, 401 (2001).
[94] M. Diehl, Phys. Rep. **388**, 41 (2003).
[95] A. V. Belitsky and A. V. Radyushkin, Phys. Rep. **418**, 1 (2005).
[96] S. Boffi and B. Pasquini, Riv. Nuovo Cimento **30**, 387 (2007).
[97] X. Ji, Annu. Rev. Nucl. Part. Sci. **54**, 413 (2004).
[98] X. D. Ji, Phys. Rev. D **55**, 7114 (1997).
[99] S. J. Brodsky, D. Chakrabarti, A. Harindranath, A. Mukherjee, and J. P. Vary, Phys. Rev. D **75**, 014003 (2007).
[100] A. V. Radyushkin, Phys. Rev. D **56**, 5524 (1997).
[101] M. Burkardt, Phys. Rev. D **62**, 071503 (2000); **66**, 119903(E) (2002).
[102] M. Diehl, Eur. Phys. J. C **25**, 223 (2002); **31**, 277(E) (2003).
[103] D. Chakrabarti and A. Mukherjee, Phys. Rev. D **72**, 034013 (2005).
[104] P. Hagler, A. Mukherjee, and A. Schafer, Phys. Lett. B **582**, 55 (2004).
[105] K. Kanazawa, C. Lorcé, A. Metz, B. Pasquini, and M. Schlegel, Phys. Rev. D **90**, 014028 (2014).
[106] A. Rajan, A. Courtoy, M. Engelhardt, and S. Liuti, Phys. Rev. D **94**, 034041 (2016).
[107] C. Lorcé and B. Pasquini, J. High Energy Phys. 09 (2013) 138.
[108] S. Sharma and H. Dahiya, Eur. Phys. J. A **59**, 235 (2023).
[109] S. Chekanov *et al.* (ZEUS Collaboration), Phys. Lett. B **573**, 46 (2003).
[110] ZEUS Collaboration, J. High Energy Phys. 05 (2009) 108.
[111] F. X. Girod *et al.* (CLAS Collaboration), Phys. Rev. Lett. **100**, 162002 (2008).
[112] G. Gavalian *et al.* (CLAS Collaboration), Phys. Rev. C **80**, 035206 (2009).
[113] S. Niccolai (CLAS Collaboration), Proc. Sci. QNP2012 (**2012**) 053 [arXiv:1207.3191].
[114] S. Pisano *et al.* (CLAS Collaboration), Phys. Rev. D **91**, 052014 (2015).
[115] H. S. Jo *et al.* (CLAS Collaboration), Phys. Rev. Lett. **115**, 212003 (2015).
[116] N. Hirlinger Saylor *et al.* (CLAS Collaboration), Phys. Rev. C **98**, 045203 (2018).
[117] M. Hattawy *et al.* (CLAS Collaboration), Phys. Rev. Lett. **123**, 032502 (2019).
[118] V. Burkert *et al.* (CLAS Collaboration), Eur. Phys. J. A **57**, 186 (2021).
[119] K. Kumericki, S. Liuti, and H. Moutarde, Eur. Phys. J. A **52**, 157 (2016).
[120] V. Bertone, H. Dutrieux, C. Mezrag, H. Moutarde, and P. Sznajder, Phys. Rev. D **103**, 114019 (2021).
[121] E. Moffat, A. Freese, I. Cloët, T. Donohoe, L. Gamberg, W. Melnitchouk, A. Metz, A. Prokudin, and N. Sato, Phys. Rev. D **108**, 036027 (2023).
[122] C. Lorcé, Phys. Lett. B **735**, 344 (2014).
[123] A. Bhoonah and C. Lorcé, Phys. Lett. B **774**, 435 (2017).
[124] M. Burkardt, Int. J. Mod. Phys. A **18**, 173 (2003).
[125] S. J. Brodsky, H. C. Pauli, and S. S. Pinsky, Phys. Rep. **301**, 299 (1998).
[126] A. Harindranath, arXiv:hep-ph/9612244.
[127] T. Maji and D. Chakrabarti, Phys. Rev. D **94**, 094020 (2016).
[128] D. Chakrabarti, N. Kumar, T. Maji, and A. Mukherjee, Eur. Phys. J. Plus **135**, 496 (2020).
[129] T. Maji and D. Chakrabarti, Phys. Rev. D **95**, 074009 (2017).
[130] B. Gurjar, D. Chakrabarti, and C. Mondal, Phys. Rev. D **106**, 114027 (2022).
[131] D. Chakrabarti, C. Mondal, A. Mukherjee, S. Nair, and X. Zhao, Phys. Rev. D **102**, 113011 (2020).
[132] S. Sharma, N. Kumar, and H. Dahiya, Nucl. Phys. **B992**, 116247 (2023).
[133] S. Sharma and H. Dahiya, Int. J. Mod. Phys. A **37**, 2250205 (2022).
[134] S. Sharma, S. Jain, and H. Dahiya, Phys. Rev. D **110**, 074025 (2024).
[135] T. Maji, C. Mondal, and D. Kang, Phys. Rev. D **105**, 074024 (2022).

[136] S. Sharma and H. Dahiya, Nucl. Phys. **B1001**, 116522 (2024).
[137] T. Maji, C. Mondal, and D. Chakrabarti, Phys. Rev. D **96**, 013006 (2017).
[138] J. R. Ellis, D. S. Hwang, and A. Kotzinian, Phys. Rev. D **80**, 074033 (2009).
[139] G. P. Lepage and S. J. Brodsky, Phys. Rev. D **22**, 2157 (1980).
[140] G. F. de Teramond and S. J. Brodsky, arXiv:1203.4025.
[141] S. J. Brodsky and G. F. de Teramond, Phys. Rev. D **77**, 056007 (2008).
[142] T. Gutsche, V. E. Lyubovitskij, I. Schmidt, and A. Vega, Phys. Rev. D **91**, 054028 (2015).
[143] A. V. Efremov, P. Schweitzer, O. V. Teryaev, and P. Zavada, Phys. Rev. D **80**, 014021 (2009).
[144] M. Burkardt, arXiv:0709.2966.
[145] D. Chakrabarti and C. Mondal, Eur. Phys. J. C **73**, 2671 (2013).
[146] D. Chakrabarti and C. Mondal, Phys. Rev. D **88**, 073006 (2013).
[147] S. Meissner, A. Metz, and M. Schlegel, J. High Energy Phys. 08 (2009) 056.
[148] Z. Zhang, Z. Hu, S. Xu, C. Mondal, X. Zhao, and J. P. Vary (BLFQ Collaboration), Phys. Rev. D **109**, 034031 (2024).
[149] S. Bhattacharya, K. Cichy, M. Constantinou, J. Dodson, X. Gao, A. Metz, J. Miller, S. Mukherjee, P. Petreczky, F. Steffens *et al.*, Phys. Rev. D **109**, 034508 (2024).
[150] M. Burkardt, Phys. Rev. D **62**, 071503 (2000); **66**, 119903(E) (2002).